

1 **High throughput screening identifies SOX2 as a Super Pioneer Factor that**
2 **inhibits DNA methylation maintenance at its binding sites.**

3 Ludovica Vanzan¹, Hadrien Soldati^{1§}, Victor Ythier¹, Santosh Anand¹, Nicole Francis²,
4 Rabih Murr^{1,3*}

5 *¹Department of Genetic Medicine and Development, University of Geneva Medical*
6 *School, Geneva, Switzerland.*

7 *²Institut de Recherches Cliniques de Montréal (IRCM) and Département de biochimie*
8 *et médecine moléculaire, Université de Montréal, Montréal, Canada.*

9 *³Institute for Genetics and Genomics in Geneva (iGE3), University of Geneva,*
10 *Geneva, Switzerland*

11 *[§]Present address: Department of Physiology and Metabolism, University of Geneva*
12 *Medical School, Geneva, Switzerland*

13

14 *Correspondence: R. Murr. Department of Genetic Medicine and Development
15 (GEDEV), University of Geneva, Medical School, 1 Rue Michel-Servet, Geneva 1206,
16 Switzerland

17 rabih.murr@unige.ch

18

19 **Abstract**

20 Access of mammalian transcription factors (TFs) to regulatory regions, an essential
21 event for transcription regulation, is hindered by chromatin compaction involving
22 nucleosome wrapping, repressive histone modifications and DNA methylation.

23 Moreover, methylation of TF binding sites (TBSs) affects TF binding affinity to these
24 sites. Remarkably, a special class of TFs called pioneer transcription factors (PFs)
25 can access nucleosomal DNA, leading to nucleosome remodelling and chromatin
26 opening. However, whether PFs can bind to methylated sites and induce DNA
27 demethylation is largely unknown.

28 Here, we set up a highly parallelized approach to investigate PF ability to bind
29 methylated DNA and induce demethylation. Our results indicate that the
30 interdependence between DNA methylation and TF binding is more complex than
31 previously thought, even within a select group of TFs that have a strong pioneering
32 activity; while most PFs do not induce changes in DNA methylation at their binding
33 sites, we identified PFs that can protect DNA from methylation and PFs that can
34 induce DNA demethylation at methylated binding sites. We called the latter “super
35 pioneer transcription factors” (SPFs), as they are seemingly able to overcome
36 several types of repressive epigenetic marks. Importantly, while most SPFs induce
37 TET-dependent active DNA demethylation, SOX2 binding leads to passive
38 demethylation by inhibition of the maintenance methyltransferase DNMT1 during
39 replication. This important finding suggests a novel mechanism allowing TFs to
40 interfere with the epigenetic memory during DNA replication.

41

42

43 **Introduction**

44 Transcription factor (TF) binding to specific sites at gene-proximal and -distal
45 regulatory regions is a fundamental step in gene expression regulation. However, as
46 the sequence of a given regulatory region is similar in all cells, the regulation of cell-
47 specific transcription is likely to depend on non-genetic regulators. Indeed, TF
48 access to regulatory elements is controlled by the chromatin structure, which in turn
49 is modulated by epigenetic modifications (nucleosome remodelling, histone
50 modifications and DNA methylation). These are classified into active or repressive
51 according to their effect on gene expression. DNA tightly wrapped around
52 nucleosomes due to repressive histone marks was shown to be refractory to TF
53 binding¹. Therefore, activity of nucleosome remodellers to open the chromatin was
54 deemed necessary prior to TF binding to compact chromatin². However, several
55 studies identified a new class of TFs, called pioneer transcription factors (PFs) that
56 access their target sites in condensed chromatin. This results in chromatin “de-
57 condensation” by nucleosome remodelling, recruitment of “settler” TFs that are
58 unable to access condensed chromatin, and transcription activation³⁻⁶. These
59 findings hint for a more complex relationship between epigenetic- and genetic-based
60 mechanisms in transcription regulation than previously thought. It is therefore
61 important to establish whether and when epigenetic mechanisms constitute a
62 primary event in the regulation of transcription and when do they simply result from
63 previous events governed by the genetic composition of the regulatory regions (i.e.
64 TF binding).

65 DNA methylation is an essential epigenetic modification that was hypothesized not
66 only to inhibit the accessibility of DNA but also its affinity to TFs^{7,8}. Remarkably,
67 recent studies have shown that not all TFs show sensitivity to DNA methylation.

68 Moreover, some TFs were shown to preferentially bind to methylated sites^{9–11}.
69 However, it is currently less clear whether TFs, notably those that can bind to
70 methylated DNA, lead to changes in the methylation status of their binding sites (i.e.
71 DNA demethylation), and if so, how. More precisely, can PFs, in addition to their
72 ability to remodel the nucleosomes, induce DNA demethylation?
73 Using a high throughput approach, our study methodically determined the ability of
74 reported PFs to induce DNA demethylation at their binding sites in mouse embryonic
75 stem cells (ESCs) and *in vitro* differentiated neuronal progenitors (NPs). Results
76 show that, while many PFs do not affect the methylation status of their binding sites,
77 a group of PFs that we call “protective pioneer transcription factors (PPFs)” protect
78 DNA from *de novo* acquisition of methylation, while another group called “super
79 pioneer transcription factors (SPFs)” induce DNA demethylation at their methylated
80 binding sites. Importantly, we show that most SPF-driven demethylation is TET-
81 dependent, except for SOX2 that inhibits DNMT1 at the replication fork, thus leading
82 to replication-dependent passive DNA demethylation.

83 **Results:**

84 **Hi-TransMet: a high throughput assay for the analysis of transcription factor**
85 **binding effect on DNA methylation**

86 We developed a method called Hi-TransMet (for high throughput analysis of
87 transcription factor effect on DNA methylation) that allows to assess the effect of up
88 to hundreds of transcription factors (TFs) on DNA methylation around their binding
89 sites, in parallel. The method is based on bisulfite deep sequencing of PCR
90 amplicons of the same sequence backbone with known methylation status but
91 containing different TF binding motifs. Specifically, we used a transgenic mouse ESC
92 line, in which a targeting site surrounded by two inverted LoxP sites, was engineered
93 at the β -globin locus¹²⁻¹⁴. This locus is inactive in non-erythroid cells and was shown
94 to not interfere with the methylation status of the cassette. Using the Recombinase-
95 Mediated Cassette Exchange (RMCE) approach¹⁵, we could replace the cassette
96 with any DNA fragment surrounded by two LoxP sites in a donor plasmid
97 (**supplementary figure 1a**). In particular, we chose as a backbone a bacterial DNA
98 fragment (FR1, **supplementary figure 1b**) with a CpG ratio of 3.6%, making it a
99 CpG island akin to an intermediate CpG-content promoter (ICP)¹⁶. FR1 was reported
100 to get fully methylated, when inserted in the RMCE site either unmethylated or *in*
101 *vitro* methylated (M.SssI methyltransferase treatment). Importantly, the fragment is
102 unlikely to contain any mammalian TF motif due to evolutionary distance to
103 mammals¹², thus inclusion of a TF binding motif within it could address whether the
104 corresponding TF can protect DNA from methylation or induce DNA demethylation.
105 Moreover, using the same genetic backbone reduces TF-independent background
106 interference, while using unique molecular barcoding removes bisulfite PCR
107 amplification biases.

108 **Validation of Hi-TransMet to study the effect of major pioneer transcription**
109 **factors on DNA methylation at their binding sites**

110 With the aim of identifying factors that can lead to protection from *de novo*
111 methylation or to DNA demethylation, we focused on PFs, as their ability to access
112 nucleosomal DNA in compact chromatin makes them ideal candidates for binding
113 methylated DNA and affecting the methylation status. Twenty-seven PFs were
114 selected based on previously published reports of pioneering activity. Moreover,
115 selected PFs, with the exception of ER α used as a negative control, are expressed
116 in mESCs or in neuronal progenitors (NPs) derived by *in vitro* differentiation of
117 mESCs (**supplementary table 1**)¹⁷. Consensus wild-type (WT) binding motifs were
118 extracted from public databases^{18–20} or from studies that used ChIP-Seq data for *de*
119 *novo* motif identification^{21,22}. One binding motif was selected for every TF with a few
120 exceptions: GATA3, 4 and 6 share the same binding motif. SOX2 motif was
121 introduced either alone or in combination with the OCT4 motif as the two factors
122 were shown to often colocalize both in ESCs^{23–25} and during differentiation²⁶. Two
123 reported CTCF motifs (CTCF.1 and CTCF.2) corresponding to two different
124 directionalities were included, as the direction of CTCF motif was reported to affect
125 its looping direction²⁷ (**supplementary tables 1 and 2**). For each WT motif, we
126 designed a scrambled (Sc) control motif (**supplementary table 2**) with a significantly
127 weaker binding score and in which all CpG positions present in their WT
128 counterparts are maintained. Additionally, we assigned six base pair barcodes on
129 either side of each motif (**figure 1a**). One strand of these barcodes does not contain
130 cytosines and is therefore not affected by bisulfite treatment, thus facilitating motif
131 recognition following bisulfite conversion. We designed the “barcode-motif-barcode”
132 combination by avoiding any resemblance to known TF motifs other than the ones

133 intended (**supplementary table 2**).

134 Double-stranded DNA oligomers each representing a unique motif-barcode
135 combination were individually cloned into the FR1 within the RMCE donor plasmid
136 (**supplementary figure 1b**). Plasmids, each containing FR1, one motif and one
137 barcode, were mixed equimolarly to generate the targeting library that was further
138 divided into 2 libraries: one was *in vitro* methylated (+ Sssl), while the second did not
139 undergo any further treatment (- Sssl). Libraries were separately transfected into the
140 transgenic mESCs, together with a plasmid expressing the CRE recombinase
141 (**figure 1a**). Genomic DNA was then extracted from successfully recombinant cells
142 and treated with sodium bisulfite, followed by amplification of the RMCE site using an
143 approach that amplifies the site regardless of the identity of the inserted motif and
144 labels each molecule with a unique molecular identifier (UMI)²⁸. This allows
145 quantifying the methylation of the original unamplified sequences exclusively
146 (**supplementary figure 2a and 2b**). Reduction of methylation at CpGs surrounding
147 WT binding motifs in comparison to those around the corresponding Sc motifs allows
148 to identify PFs protecting DNA from methylation (-Sssl condition) or inducing DNA
149 demethylation (+Sssl condition) (**figure 1b**).

150 To verify the functionality of Hi-TransMet and its ability to correctly identify factors
151 whose putative binding could lead to lower methylation, we checked the methylation
152 levels of the FR1 fragment including CTCF.1 WT and Sc motifs, as a similar
153 experimental setting was used to study CTCF-mediated DNA demethylation¹⁴. For
154 this experiment, we used transgenic ESC lines that include FR1 with individual
155 CTCF motifs. The results show that CTCF binding can both protect unmethylated
156 sites from acquisition of *de novo* methylation (-Sssl condition) and induce
157 demethylation at methylated sites (+Sssl condition). CTCF binding at WT motifs and

158 its absence at Sc motifs were verified by chromatin immunoprecipitation (ChIP)
159 (**figure 1d**). These results validate the use of Hi-TransMet to identify factors that
160 protect DNA from *de novo* methylation or induce DNA demethylation.

161 **Identification of pioneer transcription factors that can protect DNA against *de*** 162 ***novo* methylation at their binding sites**

163 To identify factors that can protect DNA from *de novo* methylation, we analysed
164 reads generated by Hi-TransMet performed under -SssI condition in ESCs. After
165 sorting reads according to their motif-barcode combination, methylation percentages
166 was extracted for all CpGs 300 bp upstream and 250 bp downstream of the inserted
167 motifs (**supplementary figure 2b**). Methylation levels around WT and Sc motifs
168 were first independently analysed (**figure 2a**). As previously reported¹², the
169 fragments become methylated upon insertion, although not completely, with an
170 average CG methylation level of 52.4% around Sc motifs (**figure 2a** and
171 **supplementary figure 3**). Moreover, while lower methylation levels are observed
172 mostly around WT motifs, there are also changes related to Sc motifs and therefore
173 unrelated to the binding of tested PFs. To correct for this, we subtract, for every
174 motif, the methylation level of each CpG in the locus with the Sc motif from that of
175 the same CpG in the locus with the WT motif ($\Delta\text{met} = \% \text{met_WT} - \% \text{met_Sc}$,
176 **figure 2b**). Only significantly lower methylation in WT than in Sc conditions will be
177 considered as directly related to PF binding. We then classified different effects of TF
178 motifs on DNA methylation using unsupervised hierarchical clustering, followed by
179 the identification of statistically significant hypomethylated regions in WT conditions
180 (HMRs). HMRs are defined as regions of more than 50bp and containing a minimum
181 of 3 consecutive CpGs, each having a Δmet of 10% or higher.

182 Results show that PFs differ in their ability to protect DNA from methylation. Globally,
183 it seems that, upon binding, only few of the selected PFs can protect from *de novo*
184 DNA methylation. We called these “protective pioneer factors (PPFs)”. In addition to
185 the previously reported^{14,30} CTCF (CTCF.1 and CTCF.2) and NRF1, our results
186 indicate that also KLF4, KLF7, OCT4-SOX2, SOX9, REST, OTX2, and E2F1 protect
187 against methylation (**figure 2b**). Moreover, SOX2 alone, but not OCT4, seems to be
188 able to protect against methylation, although this ability is increased in the presence
189 of a combined OCT4-SOX2 motif. It is important to note that all identified PPFs, with
190 the exception of SOX9, are highly expressed in ESCs (**figure 2c**).

191 **Identification of super pioneer transcription factors that can induce DNA** 192 **demethylation at their binding sites**

193 To identify PFs that can cause DNA demethylation upon binding to methylated DNA
194 in ESCs, we analysed methylation levels in the +Sssl condition. The inserted
195 fragment maintained high levels of methylation in ESCs, with an average CG
196 methylation level of 79.1% in fragments with Sc motifs (**figure 3a** and
197 **supplementary figure 3a**). Under these conditions, we observed extensive DNA
198 demethylation around the binding sites of several factors: CTCF (CTCF.1 and
199 CTCF.2), REST, KLF4, OCT4-SOX2, SOX9, SOX17, E2F1, N-MYC, and GR.
200 Moreover, there is again a considerable reduction of DNA methylation around the
201 SOX2 motif, while this is less apparent around OCT4 motif (**figure 3b**). We called
202 the corresponding factors “super pioneer transcription factors (SPFs)” as, in addition
203 to their known ability to induce chromatin remodelling, they are also able to induce
204 DNA demethylation (**figure 2c**). It is interesting to note that CTCF, REST, SOX2,
205 SOX9, E2F1 and KLF4 TFs both protect from *de novo* methylation and induce DNA
206 demethylation. On the other hand, NRF1 and OTX2, can only protect DNA from

207 methylation but have no effect on methylated DNA. This is in concordance with a
208 previously published study defining NRF1 as methylation sensitive³⁰. Similar to
209 PPFs, most SPFs, with the exception of SOX9 and SOX17, are highly expressed in
210 ESCs.

211 Interestingly, clustering of the results revealed that reduction in DNA methylation at
212 some PPF and SPF binding sites extends far beyond the TF binding site. This could
213 be due to the sequence context of our reporter DNA fragment, which lacks motifs for
214 other TFs, but might also suggest more active mechanisms, rather than steric
215 hindrance, used by PFs to maintain low levels of DNA methylation and render a
216 large region available for the binding of settler TFs.

217 **PPFs and SPFs are cell-type specific**

218 PPF- and SPF-mediated effects on DNA methylation are expected to be dynamic
219 during differentiation as a function of cell-type-specific TF expression. Therefore, we
220 differentiated the transgenic ESCs into neuronal progenitors (NPs)¹⁷, in order to both
221 confirm our results in ESCs and identify new NP-specific PPFs and SPFs.

222 Comparison of gene expression profiles derived by RNA-Seq data in ESCs and NPs
223 highlighted the differences in expression of the tested PFs between the two cell
224 types (**figures 4a** and **4b**). Hi-TransMet was then performed in NPs and methylation
225 levels around PF motifs in ESCs and NPs were compared. First, differential
226 expression of each tested PF in ESCs and NPs was plotted against the difference in
227 Δmet between ESCs and NPs ($\Delta\Delta\text{met} = \Delta\text{met ESCs} - \Delta\text{met NPs}$) of the FR1
228 containing the corresponding PF motif. This showed an overall anticorrelation in both
229 -Sssl and +Sssl conditions (**figures 4c** and **4d**), indicating that most methylation
230 changes are indeed driven by the direct activity of the corresponding PFs.

231 Average methylation levels highly increased during differentiation, reaching 81.7%
232 (Sc motifs) in the -Sssl condition (**supplementary figures 3a** and **4a**) and 85.9% in
233 the +Sssl condition (**supplementary figures 3a** and **4b**). In the -Sssl condition,
234 statistical analysis identified HMRs around CTCF.1, CTCF. 2, REST, KLF4, OCT4-
235 SOX2, SOX9 and N-MYC binding sites (**figure 4e**). On the other hand, FR1/+Sssl
236 data analysis identified CTCF, REST, OCT4-SOX2, SOX17, CREB, FOXA1 and
237 FOXD3 as SPFs (**figures 4f** and **4g**).

238 **Most SPFs induce TET-dependent DNA demethylation**

239 Next, we sought to determine the mechanisms used by SPFs to demethylate their
240 binding sites. DNA demethylation could occur in a replication-dependent fashion
241 through the inhibition of the methylation maintenance machinery, notably the DNA
242 methyltransferase DNMT1. Another possibility is the SPF-dependent induction of
243 replication-independent active demethylation processes.

244 Ten-Eleven Translocation (TET)-dependent oxidation of 5-methylcytosine (5-mC)
245 into 5-hydroxymethylcytosine (5-hmC) is currently considered as an essential step
246 for active DNA demethylation. Several groups published interactions between PFs
247 and TET enzymes³¹⁻³⁷ (**supplementary table 1**), consistent with studies reporting
248 correlation between low levels of 5mC and high levels of 5hmC and TET proteins at
249 TF-binding sites^{31,38}.

250 To address the functional involvement of TET proteins in SPF-dependent DNA
251 demethylation, we performed Hi-TransMet on FR1/+Sssl in mESCs lacking all TET
252 proteins: TET1/2/3 triple knockout (TKO)³⁹, to study the capacity of the identified
253 SPFs to induce DNA demethylation in this context. In the absence of TET proteins,
254 average methylation levels of FR1 are significantly higher than in ESCs expressing

255 TETs, both in CG context (88.6% at Sc motifs, **figure 5a** and **supplementary figure**
256 **3a**) and non-CG context (6.3%, **supplementary figure 3b**), suggesting that TET
257 proteins are responsible for most binding-specific and unspecific demethylation
258 events observed in the previous experiments. Results show that most SPF-
259 dependent DNA demethylation activity is weak or absent in TET TKO cells,
260 indicating that most SPFs induce active DNA demethylation (**figure 5b**).
261 Interestingly, demethylation occurs in the absence of TETs at the OCT4-SOX2
262 binding site. This is also observed at the SOX2 motif alone, although no statistically
263 significant HMRs were identified. Other PF motifs that have lower methylation under
264 these conditions are FOXD3, GATA and ETS. GATA factors and ETS have very low
265 expression in ESCs although they are slightly upregulated in TET TKO cells (**figure**
266 **5c**). It is therefore unlikely that the effect we see around their corresponding motifs is
267 directly driven by these factors. On the other hand, FOXD3 is both highly expressed
268 in TET TKO cells (**figure 5c**) and shows moderate SPF activity in NPs. SOX2, and
269 FOXD3 might therefore lead to passive DNA demethylation. As TET TKO ESCs
270 cannot differentiate into NPs, NP-specific SPFs as well were included in the
271 following experiments aimed at testing SPF-dependent passive demethylation.

272 **SOX2 inhibits DNMT1 activity**

273 As maintenance of DNA methylation is catalysed by DNMT1, we set up an *in vitro*
274 methylation assay to assess the effect of PFs on DNMT1 activity⁴⁰. A double
275 stranded hemi-methylated DNA probe containing the PF motif of interest and a
276 single CpG (either within or in the immediate vicinity of the motif) was incubated with
277 DNMT1 protein and radioactively-labelled S-Adenosyl-L-methionine (SAM[3H]) as a
278 methyl donor, in the presence or absence of the corresponding PF. Integration of the
279 radioactively-labelled methyl group in the unmethylated strand was measured as a

280 readout of DNMT1 activity and for each PF, the signal in the presence of the WT
281 motif was normalized to the signal in the presence of the Sc motif.

282 Surprisingly, results showed that only SOX2, and to a lesser extent OTX2 and ETS,
283 among all tested SPFs and non-SPFs, significantly reduce DNMT1 activity (**figure**
284 **6a**). Moreover, the presence of SOX2 alone, but not OCT4, is sufficient to
285 significantly reduce DNMT1 activity on the combined OCT4-SOX2 probe, further
286 confirming that SOX2 inhibits DNMT1 activity on hemi-methylated DNA (**figure 6b**).
287 Unlike SOX2, FOXD3 does not affect DNMT1 activity. This suggests that FOXD3
288 might induce a TET-independent active demethylation. Finally, NP-specific SPFs
289 SOX17, CREB, and FOXA1 do not affect DNMT1 activity, suggesting that they
290 depend on TETs to induce demethylation.

291 **SOX2 inhibits DNA methylation maintenance during replication**

292 To address if SOX2-dependent inhibition of DNMT1 takes place during DNA
293 replication, we setup an *in vitro* replication assay^{41,42} that assesses the effect of TFs
294 on the maintenance of DNA methylation. Briefly, a bacterial DNA fragment
295 containing the tested motif is cloned into an SV40 replication vector⁴³ to generate the
296 replication substrate. Incubation of the substrate with T-Antigen (T-Ag) and cellular
297 extracts leads to its replication. Addition of biotinylated dUTP to the reaction results
298 in biotinylation of nascent DNA. Thus, Immunoprecipitation with streptavidin beads
299 enriches for newly synthesized biotinylated DNA. Complete replication is verified by
300 digestion with DpnI, an enzyme that cuts specifically at GATC sites when the
301 Adenosine is methylated. As m6A is not maintained during replication, replicated
302 templates are protected from digestion (**supplementary figure 5b**). Finally, the
303 substrate could be *in vitro* methylated by treatment with SssI prior to the replication
304 reaction, and the maintenance of methylation can be assessed by adding SAM[3H]

305 to the replication reaction and counting the integration events of the radioactive
306 methyl group or by bisulfite sequencing of the replicated product.

307 We performed the replication reaction in the presence or absence of the PF of
308 interest. PF binding to the plasmid was verified by EMSA (**supplementary figure**
309 **5c**), and SAM[3H] incorporation was measured by scintillation counting and
310 normalized to the signal in absence of PFs. Results show that the substrate
311 replicates efficiently (**supplementary figure 5d**) and replicated templates maintain
312 DNA methylation in the absence of PFs (**supplementary figure 5d and figure 6d**).
313 Unmethylated templates, and templates incubated in the absence of T-Ag (which do
314 not replicate) do not incorporate SAM[3H], confirming that SAM[3H] incorporation
315 reflects maintenance methylation. Interestingly, in the presence of SOX2 protein, we
316 observed a significant reduction in methyl group incorporation around the WT motif,
317 clearly suggesting that SOX2 interferes with the maintenance of DNA methylation
318 during replication. Moreover, analysis of the methylation status around the motifs by
319 bisulfite Sanger sequencing of replicated DNA in two independent replicates (**figure**
320 **6d and supplementary figure 5e**) confirmed a reduction in DNA methylation in the
321 presence of SOX2, but not of CTCF, FOXA1 and NFY, further suggesting that SOX2
322 recruitment leads to passive DNA demethylation by DNMT1 inhibition.

323 **Discussion:**

324 While PF effect on nucleosome compaction is well documented, PF interaction with
325 DNA methylation is still poorly addressed. Here, we established Hi-TransMet, a high-
326 throughput approach to assess the effect of TFs on DNA methylation. While we
327 focused on PF crosstalk with DNA methylation, this method could be used with any
328 DNA-binding factor of interest and the throughput can be easily increased.

329 It is important to note that all WT motifs used here were previously tested
330 experimentally for their ability to specifically and efficiently recruit their corresponding
331 TFs, either by ChIP experiments, or DNA/protein microarrays and EMSA. Therefore,
332 we made the assumption that the TFs bind to the WT motifs in our setting and
333 therefore that lower DNA methylation levels around WT motifs in comparison to
334 those around Sc motifs are linked to this binding event. This assumption was
335 validated by ChIP assays performed on selected PFs (**supplementary figure 6**).

336 Using Hi-TransMet, we identified PPFs that are able to protect against *de novo*
337 methylation. Our screening both confirms previously reported PPFs (NRF1^{30,44},
338 CTCF and REST¹⁴) and identifies new ones, either constitutive (KLF4, SOX2, SOX9)
339 or ESCs- (KLF7, E2F1 and OTX2) and NP-specific (N-MYC) (**figure 4g**). Whether
340 PPF binding shields its surrounding from DNA methyltransferases by steric
341 hindrance or whether PPFs directly interact with DNMT3a/3b/3L leading to their
342 inhibition awaits further studies. We also identified SPFs that, in addition to their
343 known pioneering activities, can induce DNA demethylation at their binding sites.
344 Constitutive SPFs are CTCF, REST, SOX2, and SOX17. ESC-specific SPFs are
345 KLF4, E2F1, GR, N-MYC and SOX9 while NP-specific SPFs are FOXA1, FOXD3,
346 and CREB (**figure 4g**).

347 Considering the previously established PF ability to access their binding sites in a

348 closed chromatin context, the identification of SPFs introduces a further level of
349 classification and suggests a clear hierarchy among TFs in the fine regulation of
350 gene expression. We propose a model where SPFs are the first to engage
351 methylated binding sites. This is followed by DNA demethylation allowing the
352 recruitment of “normal” PFs and further chromatin opening, which provides access to
353 settler TFs (**figure 7**).

354 In accordance with our results, CTCF and REST were both predicted to induce DNA
355 demethylation at their binding sites¹⁴. Similarly, several FOX factors were linked with
356 DNA demethylation and TET1^{45–48}. Moreover, overexpression of FOXA2, a paralog
357 of FOXA1, in fibroblasts correlates with chromatin opening and loss of methylation at
358 its target sites. The pluripotency factor KLF4 was also recently shown to mediate
359 active DNA demethylation at closed chromatin regions by interacting with TET2
360 during reprogramming³¹. Conversely, KLF7 was shown to interact with DNMT3a in
361 TF protein array studies^{49,50}.

362 PPF and SPF activity seems to depend not only on their expression levels, but also
363 on their interactors, PTMs, and roles in the different cell lines. For example, retinoic
364 acid (RA)-mediated NP differentiation drives CREB phosphorylation, a necessary
365 modification for its DNA binding ability, which could explain its NP-specific SPF
366 activity^{51,52}, despite its expression in both ESCs and NPs (**supplementary figure 6**).
367 While several studies have proposed CREB to be sensitive to DNA methylation^{53,54},
368 the lack of CREB phosphorylation in the assays used in those studies may explain
369 this discrepancy. Also, although expressed at similar levels, NRF1 and KLF7 lose
370 their protecting ability in NPs. This might indicate a lower efficiency in stably
371 protecting against methylation in conditions where higher levels of DNA methylation
372 are the default status, as it the case in NPs. N-MYC, on the other hand, induces

373 DNA demethylation in ESCs, but only protects against methylation in NPs,
374 suggesting that it is unable to demethylate highly methylated regions. Previous
375 reports on N-MYC are contradictory: on one hand, N-MYC was shown to be strongly
376 linked to regions harbouring H3K4me3 histone marks, therefore most likely having
377 low DNA methylation levels⁵⁵, and loss of N-MYC was associated with
378 heterochromatinization in neuronal stem cells⁵⁶. On the other hand, N-MYC was
379 reported to bind to hypermethylated regions in neuroblastoma cell lines, although
380 binding sites in this study were depleted of the E-box CACGTG that was used in our
381 study⁵⁷. While GR was previously shown to bind methylated cytosines in non-CG
382 context, its effect on DNA methylation was not assessed⁵⁸. Finally, SOX9 and
383 SOX17 have low expression levels in ESCs, but seem to behave as PPFs and SPFs
384 in these cells: while low expression levels may be sufficient for this activity, it cannot
385 be excluded that the motifs chosen might also be recognized and bound by other
386 SOX family members.

387 OCT4 and SOX2 are known to widely colocalize in the genome of ESCs^{26,59,60}, and
388 were reported to be involved in maintaining a hypomethylated state at the maternal
389 *Igf2/H19* ICR, possibly through DNA demethylation^{61,62}, or by protection from *de novo*
390 methylation⁶³, although a mechanism of action was not formally proposed. In our
391 study SOX2 shows a tendency, to act as a PPF, in both cell types, and as a SPF, in
392 ESCs. It can be hypothesized that, while SOX2 is the factor involved in mediating
393 protection from methylation and demethylation, OCT4 might stabilize SOX2 binding,
394 thus amplifying the effect on DNA methylation. Accordingly, it was recently shown
395 that OCT4 might not be essential for the generation of iPSCs from fibroblasts,
396 pointing towards a higher ranking for SOX2 in the hierarchy of OKSM activity⁶⁴. In
397 NPs, OCT4 is silenced and replaced by the related POU family member BRN2

398 (POU3F2) in its interaction with SOX2²⁴. Interestingly, the BRN2 binding motif is
399 highly similar to that of OCT4, so it is plausible to hypothesize that the SOX2-BRN2
400 interaction in NPs has a similar effect on DNA methylation.

401 Importantly, we show that SOX2 mediates replication-dependent passive
402 demethylation. Although the need for replication was reported for several TFs to
403 induce DNA demethylation¹¹¹, this is, to our knowledge, the first evidence of direct TF
404 interference with the activity of DNMT1 during replication, in mammals. However, the
405 exact mechanisms by which SOX2 mediates such an effect are yet to be elucidated.
406 Based on the current knowledge, two possible mechanisms of SOX2-mediated
407 passive DNA demethylation can be hypothesized: 1) SOX2 binding at the replication
408 fork inhibits DNMT1 activity by steric hindrance. In this model, SOX2 binding would
409 precede DNMT1 recruitment, as it was demonstrated that there is a delay in the
410 recruitment of DNMT1 to the replication fork^{65,66}. 2) SOX2 directly interacts with and
411 inhibits components of the maintenance machinery. Indeed, a weak interaction
412 between UHRF1 and SOX2 has been reported⁶⁷. Finally, it would be interesting to
413 assess the extent of this phenomenon and whether it is shared by other TFs. If it is
414 the case, this could constitute another piece of the puzzle explaining the
415 maintenance, or the lack thereof, of epigenetic modifications during replication.

416

417 **Online Methods**

418 Cell culture

419 TC-1(WT) ES cells¹² were cultivated on feeder cells or on dishes coated with 0.2%
420 porcine skin gelatin (Sigma, cat. No. G1890) in high glucose-DMEM medium
421 (Gibco™, cat. No. 31966021) supplemented with 1% NAA (Gibco™, 11140035),
422 1:1000 homemade LIF and 1.42nM beta mercaptoethanol. Differentiation into
423 neuronal progenitors was performed as previously described¹⁷. Briefly, ESCs were
424 grown for 4 days in CA medium (DMEM, 10% FBS, 1% NAA, 1.42nM beta-
425 mercaptoethanol) in non-adherent plates (Greiner, Bio-one 94/16 with vents,
426 633102), then supplemented with 5μM Retinoic Acid (Sigma, R-2625) for another 4
427 days. Medium was changed every two days.

428 Insertion of RMCE cassette in TET TKO cell lines

429 Insertion of the RMCE Hy-TK cassette into the TET TKO mouse ESCs was
430 performed as previously described¹². Briefly, 4x10⁶ cells were transfected with 100μg
431 of the pZRMCE plasmid linearized with SapI (NEB, R0569S) using the
432 Nucleofector™ 2b device and the Mouse ES cells Nucleofector™ kit (Lonza, VAPH-
433 1001). The plasmid includes a 2.4 kb and 3.1 kb homologous arms to the positions -
434 1300 upstream and +2332 downstream of the *Hbb-γ* ATG start, respectively. These
435 arms flank two inverted *LoxP* sites which, in turn, flank the selection cassette. Upon
436 transfection, positive selection of clones was done using 25μg/mL Hygromycin B
437 Gold (InvivoGen, ant-hg-1) for 12 days. Surviving colonies were picked and
438 screened for successful insertion by PCR (primer sequences in **supplementary**
439 **table 3**).

440 Recombinase Mediated Cassette Exchange (RMCE)

441 The bacterial fragment FR1 (**supplementary figure 1b**) was synthesized by
442 Invitrogen GeneArt Gene Synthesis and inserted into the RMCE donor plasmid by
443 directional cloning using the restriction enzymes BamHI (NEB, R3136S) and HindIII
444 (NEB, R3104L). Single stranded oligomers containing the motifs were synthesized
445 by ThermoFisher Scientific. For each motif, forward and reverse oligomers were
446 annealed and cloned into the FR1 fragment by directional cloning using the
447 restriction enzymes SphI (NEB, R3133L) and NheI (NEB, R3131L). To create the
448 plasmid libraries, single-motifs containing plasmids were mixed in equimolar fashion
449 and co-precipitated before RMCE or M.SssI treatment.

450 RMCE transfection was performed as previously described¹³. Cells containing the
451 Hy-TK RMCE cassette were cultured in ES medium (15% FBS) containing 25 μ g/ml
452 hygromycin for at least 10 days and split the day before transfection. Medium was
453 changed to 20% FBS ES medium 2 hours before electroporation. Cells were then
454 washed with PBS, detached and counted. 4 million cells were electroporated with
455 75 μ g of the targeting plasmid or plasmid libraries and 45 μ g of plc-CRE plasmid and
456 plated in two P10 dishes with 20% FBS ES medium, as before. Positive selection
457 with 3 μ M ganciclovir (NEB, CLSYN001) was started two days after transfection.
458 After 12 days, surviving colonies were picked and screened for correct insertion via
459 PCR (primer sequences in **supplementary table 3**).

460 Plasmid methylation by M.SssI treatment

461 When indicated, plasmid libraries were methylated before transfection using the
462 M.SssI CpG methyltransferase (NEB, M0226L) as previously described⁶⁸. Briefly,
463 100 μ g of plasmids were incubated with 1x NEBuffer 2, 32mM SAM and 22.5 μ L

464 20000 units/mL.M.SssI for 30 minutes. The reaction was then replenished with the
465 same amounts of SAM and M.SssI in a final volume of 500 μ L and incubated at 37°C
466 for another hour. Plasmid DNA was purified with phenol-chloroform and precipitated
467 with ethanol. Complete methylation of the samples was verified by digestion with
468 HpaII (NEB, R0171L), a methylation sensitive restriction enzyme, and methylation
469 insensitive MspI (NEB, R0106L) as a control.

470 Bisulfite conversion and PCR

471 Genomic DNA was extracted using the GenElute Mammalian genomic DNA
472 miniprep kit (Sigma, G1N70-1KT). Bisulfite conversion of 800ng gDNA (for Sanger
473 sequencing) or 3 μ g (for Hi-TransMet library preparation) was conducted using the
474 EZ DNA Methylation-Gold™ Kit (Zymo Research, D5006). Regions of interest were
475 amplified by PCR using the AmpliTaq Gold™ DNA Polymerase (Applied
476 Biosystems™, N8080241) and ran on a 1% agarose gel. Bisulfite PCR program:
477 95°C 15 min; 20 touch-down cycles from 61 to 51°C with 30 sec at 95°C, 30 sec
478 annealing T and 1 min at 72°C; 40 cycles of 30 sec at 95°C, 30 sec at 53°C and 1
479 min at 72°C; final extension at 72°C 15 min.

480 For Sanger sequencing, PCR products were extracted from 1% Agarose gels using
481 the GenElute Gel Extraction kit (Sigma, NA1111-1KT) and cloned into the pCR™4-
482 TOPO plasmid of the TOPO® TA Cloning® Kit for Sequencing (Invitrogen, K45750),
483 transformed into TOP10 bacteria, and plated on Agar dishes with 100 μ g/mL
484 Ampicillin. Individual bacterial colonies were picked, followed by amplification and
485 DNA extraction using the GenElute™ HP Plasmid Miniprep Kit (Sigma, NA0150-
486 1KT). Finally, the products were sequenced using the M13r primer. Results were
487 analysed using the BISMA or BiQ Analyzer online tools (<http://services.ibc.uni->

488 stuttgart.de/BDPC/BISMA/ and <https://biq-analyzer.bioinf.mpi-inf.mpg.de/>)^{69,70}.

489 Hi-TransMet Library Preparation and Sequencing

490 The UMI-based library protocol consists of 3 steps: annealing, non-barcoded
491 amplification and adapters addition (**supplementary figure 2a**). For each library,
492 3µg of bisulfite converted DNA were used as starting material. Annealing program:
493 95°C 15 min; gradual temperature decrease from 61°C to 51°C, -0.5°C/min; final
494 extension at 72°C 7 min. Annealing was performed using the AmpliTaq Gold™ DNA
495 Polymerase (Applied Biosystems™, N8080241), reaction set up according to the
496 manufacturer's protocol. Following a purification step to remove unused primers,
497 annealed DNA was subjected to a short amplification with a universal forward primer
498 and a specific reverse bisulfite primer: 95°C 10 min; 3 cycles of 95°C 15 sec, 50°C
499 30 sec, 72°C 1 min; final extension 72°C 5 min. Amplified DNA was purified of the
500 reaction mix, then sequencing adapters were added in a final amplification step:
501 95°C 15 min; 30 cycles of 95°C 15 sec and 60°C 2 min. Primer dimers were
502 eliminated in a final purification step. Library barcodes and primers are listed in
503 **supplementary tables 4 and 5**. The PCR steps were done using the Promega Go-
504 TaqG2 Hot Start Green Mastermix (Promega, M7423), set up according to
505 manufacturer's protocol, and all the purification steps using the Qiagen GenRead
506 Size Selection kit (Qiagen, 180514). Correct library size was verified using the
507 Agilent 2200 Tape Station system (Agilent, G2964AA, 5067- 5584 and 5067- 5585).
508 Libraries were sequenced using Illumina MiSeq platform generating 300 base pair
509 paired-end reads (PE300).

510 Chromatin Immunoprecipitation (ChIP)

511 ChIP was performed using the Diagenode IP-Star Compact Automated System robot

512 (Diagenode, B03000002) and the Diagenode AutoiDeal ChIP-qPCR kit standard
513 protocol (Diagenode, C01010181) on 4×10^6 cells. Sonication was performed using
514 the Diagenode Bioruptor Pico (Diagenode, B01060010) and the following conditions:
515 8 cycles of 30 sec ON and 30 sec OFF for mESCs; 10 cycles of 30 sec ON and 30
516 sec OFF for NPs. Correct DNA fragments enrichment at around 200bp was verified
517 using the Agilent 2200 Tape Station system (Agilent, G2964AA, 5067- 5584 and
518 5067- 5585) and by gel electrophoresis. Three independent biological replicates
519 were performed for each experiment. Antibody references: CTCF (Diagenode,
520 C15410210), OCT4 (Diagenode C15410305), SOX2 (Santa Cruz, sc-365823),
521 CREB (Abcam, ab31387), NRF1 (Abcam, ab55744). Primer sequences for qPCR
522 are listed in **supplementary table 3**.

523 *In vitro* methylation assay

524 Complementary single-stranded DNA (ssDNA) oligos, the forward strand containing
525 one methylated CpG dinucleotide within or directly next to the PF motif were
526 synthesized by Microsynth AG. Hemi-methylated double-stranded DNA (dsDNA)
527 probes were then produced by annealing these ssDNA oligomers. Annealed dsDNA
528 probes were quantified using the Qubit™ 3.0 Fluorometer with the Qubit™ dsDNA
529 HS Assay Kit (ThermoFischer Scientific, Q32854) and diluted to a final concentration
530 of 800nM. Reaction buffer was prepared as follows: 3 Ci/mmol SAM[3H] (Perkin
531 Elmer, NET 155V250UC), 1x methylation buffer [40mM Tris/HCl pH 7.5 (Invitrogen,
532 15504020), 10mM EDTA (Applichem, A1104-0500), 10mM DTT (Applichem,
533 A1101.0005), 0.2% Glycerol (Sigma, 49767-1L)], 0.2mg/mL BSA (Applichem,
534 A1391,0500), 1x Protease Inhibitor cocktail (ROCHE, 05056489001). 16.68 pmoles
535 of dsDNA probe were added to the buffer in three conditions: 1) buffer only; 2) buffer
536 + DNMT1; 3) buffer + DNMT1 + 1x TF protein at an equimolar concentration to the

537 probe. Samples were incubated at 37°C for 1h, then purified by phenol (Invitrogen
538 15513-039) and chloroform:IAA (Sigma, C0549-1PT) and ethanol precipitation. The
539 DNA pellets were resuspended in 20µL of TE buffer, then 15µL of the eluate were
540 placed on a filter paper and air dried, the remaining eluate was used to quantify the
541 probe concentration for normalization. The filter papers were transferred into
542 Scintillation Vials (Sigma, V6755-1000EA) with 4.5ml of Ultima Gold Scintillation
543 Liquid (Perkin Elmer, 6013151). Incorporation of ³H was measured on a Liquid
544 Scintillation Counter (Wallac, 1409) for 5min. The resulting measurements were
545 normalized to the concentration of the eluate before further normalization to the
546 baseline activity measured in the second condition containing only DNMT1.
547 Recombinant proteins used in the assay were: DNMT1 (Abcam, ab198140), KAISO
548 (Abcam, ab160762), ERα (Abcam, ab82606), NFYA (Abcam, ab131777), E2F1
549 (Abcam, ab82207), OCT4 (Abcam, ab169842), SOX2 (Abcam, ab169843), NRF1
550 (Abcam, ab132404), CTCF (Abcam, ab153114), FOXA1 (Abcam, ab98301), SOX9
551 (Abcam, ab131911), FOXD3 (Abcam, ab134848), KLF4 (Abcam, ab169841), ETS1
552 (Abcam, ab114322), KLF7 (Abcam, ab132999), NANOG (Abcam, ab134886), OTX2
553 (Abcam, ab200294), SOX17 (LSBio, LS-G69322-20), CREB (LSBio, LS-G28015-2),
554 GATA3 (LSBio, LS-G67133-20).

555 Protein production

556 Recombinant proteins used in *in vitro* replication experiments were either purchased
557 (SOX2, Abcam, ab169843) or prepared in Sf9 cells. Baculoviruses for expression of
558 Flag-NFYA, Flag-FoxA1, or Flag-CTCF were used to infect 1L of Sf9 cells for 48-72
559 hours as previously described⁷¹. Cells were collected by centrifugation and washed
560 with 5-10 volumes of PBS + 0.1mM PMSF. Cells were spun down, washed once with
561 1X PBS, and pellets were resuspended in 2-3 volumes of Buffer F (20mM Tris pH

562 8.0, 500mM NaCl, 4mM MgCl₂, 0.4mM EDTA, 20% glycerol) plus NP40 to 0.05%
563 with protease inhibitors (0.2mM PMSF, 13.5μM TLCK, 0.1μM Benzamidine, 3μM
564 Pepstatin, 55μM Phenanthroline, 1.5μM Aprotinin and 23μM Leupeptin), ZnCl₂
565 (10μM final concentration) and DTT (1mM final concentration). Cells were incubated
566 on ice for 30 min and homogenized with a total of 3*10 strokes during the incubation.
567 Extracts were centrifuged (30 min 48000 g), flash frozen, and stored at -80°C. For
568 anti-FLAG affinity purification, extracts incubated with protease inhibitors and 1-2ml
569 of packed anti-FLAG resin (M2-agarose, Sigma), then binding was allowed to
570 proceed overnight at 4°C with rotation. Beads were centrifuged (1500*g for 5 min),
571 then washed with the following series: 2x Buffer FN, 2x BC1200N, 2x BC2000N (the
572 second wash incubated for 15 min), 1x BC1200N, 1x BC600N, 1x BC300N, 1x
573 BC300. The initial washes were carried out in batch (5 min rotation followed by
574 centrifugation at 1000*g for 4 min), and beads transferred to an Econo Column (Bio-
575 Rad) at the BC2000N step. Proteins were eluted by incubation overnight with
576 0.4mg/mL FLAG peptide in BC300 with 10μM ZnCl₂ and protease inhibitors. Two
577 additional elutions (with 1h incubations) were collected. Eluted proteins were
578 concentrated using Amicon Ultra 0.5 Centrifugal filter units (10kDa MWCO)
579 (Millipore) and NP40 was added to 0.05% before aliquoting, flash freezing, and
580 storing at -80°C. Protein concentration was determined by Bradford assay, and
581 adjusted for the purity as determined on SYPRO Ruby stained SDS-PAGE gels.

582 *In vitro* DNA replication assay

583 For large scale DNA replication reactions used for bisulfite sequencing, TFs were
584 pre-bound to 100-200ng plasmid template in 60mM KCl, 12mM Hepes pH 7.9, 2mM
585 MgCl₂, 1mM DTT, 0.12mM EDTA, 12% glycerol, 0.01% NP40, and 10ng/μL DNA

586 template for 15 min at 30°C. For EMSA, 0.5µL of each reaction (5ng DNA) were
587 removed, mixed with 4µL of 50% glycerol/10mM EDTA, and loaded on a 0.8%
588 agarose (SeaKem)/0.5 X TBE gel, which was run for 90 min at 50V. Replication mix
589 was added to the remainder of the reaction. Replication mix consists of (per 100ng
590 DNA): 10µL HeLa S240 extract, 1.38µL replication cocktail (200µM each rNTP,
591 100µM dATP, dGTP, dCTP, 20µM dTTP, 40mM phospho-creatine, 1ng/µL creatine
592 kinase (Sigma), 3mM ATP, 5mM MgCl₂), 0.2µL human Topoisomerase II (TopoGen),
593 1mM DTT, 0.32µL Biotin-18-dUTP or Biotin-11-dUTP (1mM, Jena Bioscience or
594 Fisher), SAM[3H] (1µCi/100ng DNA, Perkin Elmer). Replication reactions were
595 incubated 90 min at 37°C. Replication reactions were stopped with DSB-PK (5µg/µL
596 of proteinase K (Biobasic), 1% SDS, 50mM Tris-HCl pH 8.0, 25% glycerol and
597 100mM EDTA), digested overnight at 50°C, followed by at least 30 min with RNaseA
598 (1µg/100ng DNA) at 37°C, and purified by phenol-chloroform and chloroform
599 extraction, followed by ethanol precipitation.

600 For binding to monovalent streptavidin beads (BcMag Monomeric Avidin Magnetic
601 Beads, Bioclone Inc.), 40µl of beads/750 ng reaction were prepared according to the
602 manufacturer's instructions. Briefly, beads were washed 1X with 4 volumes of ddH₂O
603 and 1X with 4 volumes of PBS. All wash and binding steps were carried out at room
604 temperature. Beads were incubated with 3 volumes of 5mM Biotin (in TE-100),
605 followed by washing with 6 volumes of 0.1M Glycine pH 2.8. Beads were then
606 washed twice with 4 volumes of TE-1000mM NaCl and added to purified DNA
607 samples. One sample volume of TE-1000 was added to increase the [NaCl] to
608 facilitate binding. Binding was carried out for at least one hour, and up to overnight
609 with continuous rotation. Beads were washed three times with TE-100 and eluted 3

610 times with 75 μ L mM Biotin in TE-100. Elutions were incubated at 50°C with vortexing
611 every 10-15 min.

612 To measure the incorporation of radioactive SAM[3H] during replication, reactions
613 were carried out as above in the presence of SAM[3H] with 100ng of template per
614 reaction; all steps were scaled down linearly. SAM[3H] incorporation was measured
615 by scintillation counting, and an aliquot of the purified DNA quantified from agarose
616 gels.

617 RNA extraction and cDNA preparation

618 RNA was extracted using the Qiagen RNeasy mini kit (Qiagen, 74104) with the
619 addition of the DNase step (RNase-free DNase set, Qiagen, 79254). RNA integrity
620 was verified by running an aliquot on a 1% agarose gel. Conversion of 1 μ g of RNA
621 to cDNA was done using the Takara PrimeScript 1st strand cDNA synthesis kit
622 (Takara, 6110A) according to manufacturer's protocol. qRT-PCR was performed
623 using the StepOnePlus qPCR by Applied Biosystems (ThermoFisher, 4376357) with
624 the Applied Biosystems SYBRTM Green PCR Mastermix (ThermoFisher, 4309155).
625 Primer sequences for qPCR are listed in **supplementary table 3**. Sequencing
626 libraries were prepared from 500ng of RNA using the TruSeq mRNA stranded kit
627 (Illumina, RS-122-2101). Molarity and quality were assessed by Qubit and Tape
628 Station. Biological replicates were barcoded and pooled at 2nM and sequenced on 2
629 lanes using the Illumina HiSeq 4000 sequencer.

630 Motif design

631 Criteria for choosing WT TF motifs were the following: 1) when available, motifs
632 identified from ChIP-Seq data were selected. 2) if no such data is available, Position
633 Frequency Matrices (PFMs) were obtained from the JASPAR Core Vertebrate 2016

634 database ¹⁸; alternatively, from the UniProbe ¹⁹ or TRANSFAC ²⁰ databases. WT
635 motifs were chosen mainly as the consensus sequence found in JASPAR database.
636 To minimize the cross-matching between motifs, we checked that the WT-core
637 motifs (e.g. GAATGTTTGT) and the combination restriction site-motif-barcode
638 (e.g. catgtaGCATGCtgagaaGAATGTTTGTtgagaaGCTAGCcatgta) did not match
639 with JASPAR motifs other than intended. This was done using the countPWM()
640 function of the R Biostrings package using min.score="90%". Scrambled (Sc) motifs
641 were created by random shuffling of the WT motif except for the CG dinucleotides.
642 The number and position of CG dinucleotides were maintained in WT and Sc motifs.
643 For example, WT: **CCG**TAGTCGA and SC: **TCG**AGCAGTC. Score and SC motif-
644 barcode combination were also checked for cross-matching with other JASPAR
645 motifs as for WT-sequences. To ascertain how closely the WT or Sc sequences
646 match with the respective motif's PFM, a "normalized score" was defined. At each
647 position in WT or Sc sequence, the probability of corresponding nucleotide in the
648 PFM was taken as the match score for that position. The average of match scores
649 for all positions was defined as "normalized score". Normalized scores of WT-
650 sequences were high (>0.7) and only those Sc motifs whose normalized score were
651 at least 0.3 lower than the corresponding WT motif, were used.

652 Library Data Processing

653 Paired-end libraries were trimmed using Trim Galore^{72,73} and reads with a quality
654 score below 20 were discarded. Demultiplexing was performed with Flexbar^{74,75},
655 using the 6bp library barcode plus 4bp of the neighbouring adapter for identification,
656 with 0 mismatches allowed. Concomitantly, reads were tagged using to the UMI-tags
657 option of Flexbar based on the 8 Unique Molecular Identifier (UMI) nucleotides that
658 follow the library barcode sequence. Prior to mapping, motifs were extracted and PE

659 reads were classified according to their motif using the *vmatchPattern* function with
660 unfixed sequences (allowing IUPAC code for CpGs inside the motifs) from the
661 BioString⁷⁶ package designed for R⁷⁷, with 0 mismatches allowed. Reads were then
662 mapped using Bowtie2⁷⁸ and Bismark⁷⁹, filtering out reads with non-CG methylation
663 below 2%. This filtering step was not performed for the libraries generated in TET
664 TKO cells as the levels of non-CG methylation was significantly higher in these cells
665 (**supplementary figure 3b**). Reads were then deduplicated based on their UMI tag
666 using the UMI_tools software⁸⁰ to remove PCR amplification biases. The percentage
667 of methylation for each CpG position was extracted using Bismark, considering a
668 minimum coverage of 10 reads (**supplementary figure 2b**). Biological and technical
669 replicates were pooled to ensure sufficient coverage upon verification by Multi-
670 Dimensional Scaling (MDS) that replicates were clustering well together⁸¹.
671 Ascending hierarchical clustering of the motifs, based on the methylation data, was
672 obtained using the *hclust* function in R.

673 RNA-Seq analysis

674 SE 50bp reads were trimmed⁸² and then mapped to the mouse reference genome
675 (GRm38.89 version from Ensembl) using the RNAseq aligner STAR⁸³ and
676 featureCounts⁸⁴ to assign reads to their genomic features. Library size normalization
677 and calculation of differential gene expression were performed using the edgeR
678 package. Genes with a normalized maximal expression of less than 1 RPKM in all
679 replicates were discarded. Fold-change and Benjamini-Hochberg corrected p-value
680 thresholds were set respectively to 3 and 1% for the differently expressed genes.

681 Statistical analysis

682 For the NGS data, methylation differences between WT and Sc for each CpG and for

683 each motif were calculated using the DSS (Dispersion shrinkage for sequencing
684 data) package^{85,86}, with thresholds for Δ meth and corrected p-value fixed
685 respectively at 10% and 5%. The percentage of methylation of each CpG was
686 smoothed with adjacent CpG to improve mean estimation. The smoothing option
687 was applied to a range of 50bp. Hypomethylated regions in WT vs Sc conditions
688 (HMRs) were defined as regions of more than 50bp and containing a minimum of 3
689 consecutive CpGs, each having a Δ met ($\%met_{WT} - \%met_{Sc}$) of 10% or higher.

690 For *in vitro* methylation assays, three biological replicates were analysed using two-
691 tailed unpaired t-test with Welch correction. *In vitro* replication results were analysed
692 by one-sample unpaired t-test.

693

694 **Acknowledgements**

695 We thank M. Lorincz (University of British Columbia-Vancouver) for providing the
696 RMCE plasmids; Ann Dean (National Institute for Diabetes and Digestive and Kidney
697 Diseases) and D. Schübeler (Friedrich Miescher Institute) for the RMCE target ES
698 cell line; R. Jaenisch (Whitehead Institute for Biomedical Research) for providing the
699 TET-TKO ES cells. We are grateful to Sylvain Lemeille for help in designing the
700 experimental approach and to Z. Herceg, T. Baubec, G. Andrey, and S. Braun for
701 helpful comments on the manuscript. Sequencing was performed at the iGE3
702 Genomic Platform of the University of Geneva. LV was supported by the iGE3.
703 Research in the laboratory of RM is funded by the SNSF grants PP00P3_150712,
704 PP00P3_179063 and PP00P3_190075, the Boninchi Foundation, Von Meissner
705 Foundation, and the Novartis Foundation for Medical-Biological research.

706 **Author Contributions:**

707 RM and LV conceived the study; LV, HS, NF and RM performed experiments and
708 analysed the results; HS and RM performed the in vitro methylation assays and
709 contributed to the other experiments; NF performed the in vitro replication assays;
710 VY performed the bioinformatic analysis; SA designed the motifs and contributed to
711 the bioinformatic analysis; LV inserted the RMCE selection cassette into the TET-
712 TKO ES cell lines; LV, VY and RM prepared the figures and wrote the manuscript
713 with input from all authors.

714

715

716

717 **References**

- 718 1. Thurman, R. E. *et al.* The accessible chromatin landscape of the human
719 genome. *Nature* **489**, 75–82 (2012).
- 720 2. Clapier, C. R., Iwasa, J., Cairns, B. R. & Peterson, C. L. Mechanisms of action
721 and regulation of ATP-dependent chromatin-remodelling complexes. *Nat. Rev.*
722 *Mol. Cell Biol.* **18**, 407–422 (2017).
- 723 3. Cirillo, L. A. & Zaret, K. S. An early developmental Transcription Factor
724 complex that is more stable on nucleosome core particles than on free DNA.
725 *Mol. Cell* **4**, 961–969 (1999).
- 726 4. Cirillo, L. A. *et al.* Opening of compacted chromatin by early developmental
727 Transcription Factors HNF3 (FoxA) and GATA-4. *Mol. Cell* **9**, 279–289 (2002).
- 728 5. Mayran, A. & Drouin, J. Pioneer Transcription Factors shape the epigenetic
729 landscape. *J. Biol. Chem.* **293**, 13795–13804 (2018).
- 730 6. Iwafuchi-Doi, M. The mechanistic basis for chromatin regulation by pioneer
731 transcription factors. *Wiley Interdiscip. Rev. Syst. Biol. Med.* e1427 (2018).
732 doi:10.1002/wsbm.1427
- 733 7. Tate, P. H. & Bird, A. P. Effects of DNA methylation on DNA-binding proteins
734 and gene expression. *Curr. Opin. Genet. Dev.* **3**, 226–231 (1993).
- 735 8. Schübeler, D. Function and information content of DNA methylation. *Nature*
736 **517**, 321–326 (2015).
- 737 9. Quenneville, S. *et al.* In embryonic stem cells, ZFP57/KAP1 recognize a
738 methylated hexanucleotide to affect chromatin and DNA methylation of
739 Imprinting Control Regions. *Mol. Cell* **44**, 361–372 (2011).

- 740 10. Hu, S. *et al.* DNA methylation presents distinct binding sites for human
741 transcription factors. *Elife* **2013**, 1–16 (2013).
- 742 11. Yin, Y. *et al.* Impact of cytosine methylation on DNA binding specificities of
743 human transcription factors. *Science* **356**, eaaj2239 (2017).
- 744 12. Lienert, F. *et al.* Identification of genetic elements that autonomously
745 determine DNA methylation states. *Nat. Genet.* **43**, 1091–1097 (2011).
- 746 13. Krebs, A. R., Dessus-Babus, S., Burger, L. & Schübeler, D. High-throughput
747 engineering of a mammalian genome reveals building principles of methylation
748 states at CG rich regions. *Elife* **3**, 1–18 (2014).
- 749 14. Stadler, M. B. *et al.* DNA-binding factors shape the mouse methylome at distal
750 regulatory regions. *Nature* **480**, 490–5 (2011).
- 751 15. Feng, Y.-Q. *et al.* Site-specific chromosomal integration in mammalian cells:
752 highly efficient CRE Recombinase-Mediated Cassette Exchange. *J. Mol. Biol.*
753 **292**, 779–785 (1999).
- 754 16. Weber, M. *et al.* Distribution, silencing potential and evolutionary impact of
755 promoter DNA methylation in the human genome. *Nat. Genet.* **39**, 457–466
756 (2007).
- 757 17. Bibel, M., Richter, J., Lacroix, E. & Barde, Y. Generation of a defined and
758 uniform population of CNS progenitors and neurons from mouse embryonic
759 stem cells. *Nat. Protoc.* (2007). doi:10.1038/nprot.2007.147
- 760 18. Mathelier, A. *et al.* JASPAR 2014: An extensively expanded and updated
761 open-access database of transcription factor binding profiles. *Nucleic Acids*
762 *Res.* **42**, 142–147 (2014).

- 763 19. Hume, M. A., Barrera, L. A., Gisselbrecht, S. S. & Bulyk, M. L. UniPROBE,
764 update 2015: New tools and content for the online database of protein-binding
765 microarray data on protein-DNA interactions. *Nucleic Acids Res.* **43**, D117–
766 D122 (2015).
- 767 20. Matys, V. *et al.* TRANSFAC(R) and its module TRANSCompel(R):
768 transcriptional gene regulation in eukaryotes. *Nucleic Acids Res.* **34**, D108–
769 D110 (2006).
- 770 21. Chen, X. *et al.* Integration of external signaling pathways with the core
771 transcriptional network in embryonic stem cells. *Cell* **133**, 1106–1117 (2008).
- 772 22. Liu, C. F. & Lefebvre, V. The transcription factors SOX9 and SOX5/SOX6
773 cooperate genome-wide through super-enhancers to drive chondrogenesis.
774 *Nucleic Acids Res.* **43**, 8183–8203 (2015).
- 775 23. Boyer, L. A. *et al.* Core transcriptional regulatory circuitry in human embryonic
776 stem cells. *Cell* **122**, 947–956 (2005).
- 777 24. Lodato, M. A. *et al.* SOX2 Co-Occupies Distal Enhancer Elements with Distinct
778 POU Factors in ESCs and NPCs to Specify Cell State. *PLoS Genet.* **9**, (2013).
- 779 25. Soufi, A. *et al.* Pioneer transcription factors target partial DNA motifs on
780 nucleosomes to initiate reprogramming. *Cell* **161**, 555–568 (2015).
- 781 26. Knaupp, A. S. *et al.* Transient and permanent reconfiguration of chromatin and
782 Transcription Factor occupancy drive reprogramming. *Cell Stem Cell* **21**, 834–
783 845 (2017).
- 784 27. Guo, Y. *et al.* CRISPR Inversion of CTCF Sites Alters Genome Topology and
785 Enhancer/Promoter Function. *Cell* **162**, 900–910 (2015).

- 786 28. Peng, Q., Satya, R. V., Lewis, M., Randad, P. & Wang, Y. Reducing
787 amplification artifacts in high multiplex amplicon sequencing by using
788 molecular barcodes. *BMC Genomics* **16**, (2015).
- 789 29. Lienert, F. *et al.* Identification of genetic elements that autonomously
790 determine DNA methylation states. *Nat. Genet.* **43**, 1091–1097 (2011).
- 791 30. Domcke, S. *et al.* Competition between DNA methylation and transcription
792 factors determines binding of NRF1. *Nature* **528**, 575–579 (2015).
- 793 31. Sardina, J. L. *et al.* Transcription Factors drive Tet2-mediated enhancer
794 demethylation to reprogram cell fate. *Cell Stem Cell* **23**, 1–15 (2018).
- 795 32. Costa, Y. *et al.* NANOG-dependent function of TET1 and TET2 in
796 establishment of pluripotency. *Nature* **495**, 370–374 (2013).
- 797 33. Zampieri, M. *et al.* ADP-ribose polymers localized on Ctfp-Parp1-Dnmt1
798 complex prevent methylation of Ctfp target sites. *Biochem. J.* **441**, 645–52
799 (2012).
- 800 34. Dubois-Chevalier, J. *et al.* A dynamic CTCF chromatin binding landscape
801 promotes DNA hydroxymethylation and transcriptional induction of adipocyte
802 differentiation. *Nucleic Acids Res.* **42**, 10943–10959 (2014).
- 803 35. de la Rica, L. *et al.* PU.1 target genes undergo Tet2-coupled demethylation
804 and DNMT3b-mediated methylation in monocyte-to-osteoclast differentiation.
805 *Genome Biol.* **14**, 1–21 (2013).
- 806 36. Liu, S. *et al.* Interplay of RUNX1/MTG8 and DNA methyltransferase 1 in acute
807 myeloid leukemia. *Cancer Res.* **65**, 1277–1284 (2005).
- 808 37. Goyal, S. *et al.* RUNX1 induces DNA replication independent of active DNA

- 809 demethylation at SPI1 regulatory regions. *BMC Mol. Biol.* **18**, 1–7 (2017).
- 810 38. Feldmann, A. *et al.* Transcription factor occupancy can mediate active turnover
811 of DNA methylation at regulatory regions. *PLoS Genet.* **9**, (2013).
- 812 39. Dawlaty, M. M. *et al.* Loss of TET enzymes compromises proper differentiation
813 of embryonic stem cells. *Dev. Cell* **29**, 102–111 (2014).
- 814 40. Lee, B., Morano, A., Porcellini, A. & Muller, M. T. GADD45 inhibition of DNMT1
815 dependent DNA methylation during homology directed DNA repair. *Nucleic*
816 *Acids Res.* **40**, 2481–2493 (2012).
- 817 41. Francis, N. J., Follmer, N. E., Simon, M. D., Aghia, G. & Butler, J. D. Polycomb
818 proteins remain bound to chromatin and DNA during DNA replication in vitro.
819 *Cell* **49**, 1841–1850 (2009).
- 820 42. Shimamura, S. & Ishikawa, F. Interaction between DNMT1 and DNA
821 replication reactions in the SV40 in vitro replication system. *Cancer Sci.* **99**,
822 1960–1966 (2008).
- 823 43. Stillman, B. W. & Gluzman, Y. Replication and supercoiling of simian virus 40
824 DNA in cell extracts from human cells. *Mol. Cell. Biol.* **5**, 2051–60 (1985).
- 825 44. Gebhard, C. *et al.* General transcription factor binding at CpG islands in
826 normal cells correlates with resistance to de novo DNA methylation in cancer
827 cells. *Cancer Res.* **70**, 1398–1407 (2010).
- 828 45. Yang, Y. A. *et al.* FOXA1 potentiates lineage-specific enhancer activation
829 through modulating TET1 expression and function. *Nucleic Acids Res.* **44**,
830 8153–8164 (2016).
- 831 46. Sérandour, A. A. *et al.* Epigenetic switch involved in activation of pioneer factor

- 832 FOXA1-dependent enhancers. *Genome Res.* **21**, 555–565 (2011).
- 833 47. Zhang, Y. *et al.* Nucleation of DNA repair factors by FOXA1 links DNA
834 demethylation to transcriptional pioneering. *Nat. Genet.* **48**, 1003–1013 (2016).
- 835 48. Xu, J. *et al.* Transcriptional competence and the active marking of tissue-
836 specific enhancers by defined transcription factors in embryonic and induced
837 pluripotent stem cells. *Genes Dev.* **23**, 2824–2838 (2009).
- 838 49. Hervouet, E., Nadaradjane, A., Gueguen, M., Vallette, F. M. & Cartron, P.-F.
839 Kinetics of DNA methylation inheritance by the Dnmt1-including complexes
840 during the cell cycle. *Cell Div.* **7**, 5 (2012).
- 841 50. Pacaud, R. *et al.* DNMT3L interacts with transcription factors to target
842 DNMT3L/DNMT3B to specific DNA sequences: Role of the
843 DNMT3L/DNMT3B/p65-NFκB complex in the (de-)methylation of TRAF1.
844 *Biochimie* **104**, 36–49 (2014).
- 845 51. Shan, Z. Y. *et al.* pCREB is involved in neural induction of mouse embryonic
846 stem cells by RA. *Anat. Rec.* **291**, 519–526 (2008).
- 847 52. Merz, K., Herold, S. & Lie, D. C. CREB in adult neurogenesis - master and
848 partner in the development of adult-born neurons? *Eur. J. Neurosci.* **33**, 1078–
849 1086 (2011).
- 850 53. Zhang, X. *et al.* Genome-wide analysis of cAMP-response element binding
851 protein occupancy, phosphorylation, and target gene activation in human
852 tissues. *Proc. Natl. Acad. Sci. U. S. A.* **102**, 4459–64 (2005).
- 853 54. Mann, I. K. *et al.* CG methylated microarrays identify a novel methylated
854 sequence bound by the CEBPB|ATF4 heterodimer that is active in vivo.
855 *Genome Res.* **23**, 988–997 (2013).

- 856 55. Cotterman, R. *et al.* N-Myc regulates a widespread euchromatic program in the
857 human genome partially independent of its role as a classical transcription
858 factor. *Cancer Res.* **68**, 9654–9662 (2008).
- 859 56. Knoepfler, P. S., Cheng, P. F. & Eisenman, R. N. N-myc is essential during
860 neurogenesis for the rapid expansion of progenitor cell populations and the
861 inhibition of neuronal differentiation. *Genes Dev.* **16**, 2699–2712 (2002).
- 862 57. Murphy, D. M. *et al.* Global MYCN transcription factor binding analysis in
863 neuroblastoma reveals association with distinct E-box motifs and regions of
864 DNA hypermethylation. *PLoS One* **4**, (2009).
- 865 58. Jin, J. *et al.* The effects of cytosine methylation on general transcription
866 factors. *Sci. Rep.* **6**, 1–13 (2016).
- 867 59. Boyer, L. A. *et al.* Polycomb complexes repress developmental regulators in
868 murine embryonic stem cells. *Nature* **441**, 349–353 (2006).
- 869 60. Soufi, A., Donahue, G. & Zaret, K. S. Facilitators and impediments of the
870 pluripotency reprogramming factors' initial engagement with the genome. *Cell*
871 **151**, 994–1004 (2012).
- 872 61. Hori, N., Yamane, M., Kouno, K. & Sato, K. Induction of DNA demethylation
873 depending on two sets of Sox2 and adjacent Oct3/4 binding sites (Sox-Oct
874 motifs) within the mouse H19/insulin-like growth factor 2 (Igf2) imprinted
875 control region. *J. Biol. Chem.* **287**, 44006–44016 (2012).
- 876 62. Zimmerman, D. L., Boddy, C. S. & Schoenherr, C. S. Oct4/Sox2 binding sites
877 contribute to maintaining hypomethylation of the maternal Igf2/H19 imprinting
878 control region. *PLoS One* **8**, (2013).
- 879 63. Sakaguchi, R., Okamura, E., Matsuzaki, H., Fukamizu, A. & Tanimoto, K. Sox-

- 880 Oct motifs contribute to maintenance of the unmethylated H19 ICR in YAC
881 transgenic mice. *Hum. Mol. Genet.* **22**, 4627–4637 (2013).
- 882 64. Velychko, S. *et al.* Excluding Oct4 from Yamanaka Cocktail Unleashes the
883 Developmental Potential of iPSCs. *Cell Stem Cell* 1–17 (2019).
884 doi:10.1016/j.stem.2019.10.002
- 885 65. Gruenbaum, Y., Szyf, M., Cedar, H. & Razin, a. Methylation of replicating and
886 post-replicated mouse L-cell DNA. *Proc. Natl. Acad. Sci. U. S. A.* **80**, 4919–21
887 (1983).
- 888 66. Pradhan, S., Bacolla, A., Wells, R. D. & Roberts, R. J. Recombinant Human
889 DNA (Cytosine-5) Methyltransferase. *J. Biol. Chem.* **276**, 18605–18613 (2001).
- 890 67. Kim, K. Y. *et al.* Uhrf1 regulates active transcriptional marks at bivalent
891 domains in pluripotent stem cells through Setd1a. *Nat. Commun.* **9**, (2018).
- 892 68. Schubeler, D., Lorincz, M. C. & Groudine, M. Targeting silence: the use of site-
893 specific recombination to introduce in vitro methylated DNA into the genome.
894 *Sci. Signal.* **2001**, p11 (2001).
- 895 69. Rohde, C., Zhang, Y., Reinhardt, R. & Jeltsch, A. BISMA - Fast and accurate
896 bisulfite sequencing data analysis of individual clones from unique and
897 repetitive sequences. *BMC Bioinformatics* **11**, (2010).
- 898 70. Bock, C., Reither, S., Mikeska, T., Paulsen, M. & Lengauer, T. BiQ Analyser:
899 visualization and quality control for DNA methylation data from bisulfite
900 sequencing. *Bioinformatics* **21**, 4067–8 (2005).
- 901 71. Müller, J. *et al.* Histone Methyltransferase Activity of a Drosophila Polycomb
902 Group Repressor Complex decisions are made by transiently acting
903 transcription. *Cell* **111**, 197–208 (2002).

- 904 72. Krueger, F. Babraham Bioinformatics Institute, Trim_galore. (2017).
- 905 73. Martin, M. Cutadapt removes adapter sequences from high-throughput
906 sequencing reads. *EMBnet.journal* **17**, 10–12 (2011).
- 907 74. Roehr, J. T., Dieterich, C. & Reinert, K. Flexbar 3.0 - SIMD and multicore
908 parallelization. *Bioinformatics* **33**, 2941–2942 (2017).
- 909 75. Dodt, M., Roehr, J., Ahmed, R. & Dieterich, C. FLEXBAR—Flexible Barcode
910 and Adapter processing for next-generation sequencing platforms. *Biology*
911 (*Basel*). **1**, 895–905 (2012).
- 912 76. Pagès, H., Aboyoun, P., Gentleman, R. & DebRoy, S. Biostrings: efficient
913 manipulation of biological strings. *R Packag. version 2.51.5* (2019).
- 914 77. Team, R. C. R Core Team. R: a language and environment for statistical
915 computing. *R Found. Stat. Comput. Vienna, Austria*. (2018).
- 916 78. Langmead, B. & Salzberg, S. L. Fast gapped-read alignment with Bowtie 2.
917 *Nat. Methods* **9**, 357–9 (2012).
- 918 79. Krueger, F. & Andrews, S. R. Bismark: a flexible aligner and methylation caller
919 for Bisulfite-Seq applications. *Bioinformatics* **27**, 1571–1572 (2011).
- 920 80. Smith, T. & Sudbery, I. UMI-tools: modelling sequencing errors in Unique
921 Molecular Identifiers to improve quantification accuracy. *Genome Res.* (2017).
922 doi:10.1101/gr.209601.116
- 923 81. Robinson, M. D., McCarthy, D. J. & Smyth, G. K. edgeR: A Bioconductor
924 package for differential expression analysis of digital gene expression data.
925 *Bioinformatics* **26**, 139–140 (2010).
- 926 82. Bolger, A. M., Lohse, M. & Usadel, B. Trimmomatic: a flexible trimmer for

- 927 Illumina sequence data. *Bioinformatics* **30**, 2114–2120 (2014).
- 928 83. Dobin, A. *et al.* STAR: ultrafast universal RNA-seq aligner. *Bioinformatics* **29**,
929 15–21 (2013).
- 930 84. Liao, Y., Smyth, G. K. & Shi, W. FeatureCounts: an efficient general purpose
931 program for assigning sequence reads to genomic features. *Bioinformatics* **30**,
932 923–930 (2014).
- 933 85. Feng, H., Conneely, K. N. & Wu, H. A Bayesian hierarchical model to detect
934 differentially methylated loci from single nucleotide resolution sequencing data.
935 *Nucleic Acids Res.* **42**, 1–11 (2014).
- 936 86. Wu, H. *et al.* Detection of differentially methylated regions from whole-genome
937 bisulfite sequencing data without replicates. *Nucleic Acids Res.* **43**, 1–9
938 (2015).
- 939 87. Lambert, S. A. *et al.* The Human Transcription Factors. *Cell* **172**, 650–665
940 (2018).
- 941 88. Sherwood, R. I. *et al.* Discovery of directional and nondirectional pioneer
942 transcription factors by modeling DNase profile magnitude and shape. *Nat.*
943 *Biotechnol.* **32**, 171–8 (2014).
- 944 89. Rodriguez, C. *et al.* CTCF is a DNA methylation-sensitive positive regulator of
945 the INK/ARF locus. *Biochem. Biophys. Res. Commun.* **392**, 129–134 (2010).
- 946 90. Bartke, T. *et al.* Nucleosome-interacting proteins regulated by DNA and
947 histone methylation. *Cell* **143**, 470–484 (2010).
- 948 91. Spruijt, C. G. *et al.* Dynamic readers for 5-(Hydroxy)methylcytosine and its
949 oxidized derivatives. *Cell* **152**, 1146–1159 (2013).

- 950 92. Chronis C. *et al.* Cooperative binding of Transcription Factors orchestrates
951 reprogramming. *Cell* **168**, 442–459 (2017).
- 952 93. Takahashi, K. & Yamanaka, S. Induction of pluripotent stem cells from mouse
953 embryonic and adult fibroblast cultures by defined factors. *Cell* **126**, 663–676
954 (2006).
- 955 94. Perera, A. *et al.* TET3 is recruited by REST for context-specific
956 hydroxymethylation and induction of gene expression. *Cell Rep.* **11**, 283–294
957 (2015).
- 958 95. Swinstead, E. E. *et al.* Steroid receptors reprogram FoxA1 occupancy through
959 dynamic chromatin transitions. *Cell* **165**, 593–605 (2016).
- 960 96. Dumasia, K., Kumar, A., Deshpande, S. & Balasinor, N. H. Estrogen signaling,
961 through estrogen receptor β , regulates DNA methylation and its machinery in
962 male germ line in adult rats. *Epigenetics* **12**, 476–483 (2017).
- 963 97. Thomassin, H., Flavin, M., Espinás, M. L. & Grange, T. Glucocorticoid-induced
964 DNA demethylation and gene memory during development. *EMBO J.* **20**,
965 1974–1983 (2001).
- 966 98. Huang, P. *et al.* Induction of functional hepatocyte-like cells from mouse
967 fibroblasts by defined factors. *Nature* **475**, 386–391 (2011).
- 968 99. Sekiya, S. & Suzuki, A. Direct conversion of mouse fibroblasts to hepatocyte-
969 like cells by defined factors. *Nature* **475**, 390–395 (2011).
- 970 100. Lea, A. J. *et al.* Genome-wide quantification of the effects of DNA methylation
971 on human gene regulation. *Elife* (2018). doi:10.1101/146829
- 972 101. Suzuki, T. *et al.* A screening system to identify transcription factors that induce

- 973 binding site-directed DNA demethylation. *Epigenetics and Chromatin* **10**, 1–14
974 (2017).
- 975 102. Lee, M. T. *et al.* Nanog, Pou5f1 and SoxB1 activate zygotic gene expression
976 during the maternal-to-zygotic transition. *Nature* **503**, 360–364 (2013).
- 977 103. Tsankov, A. M. *et al.* Transcription factor binding dynamics during human ES
978 cell differentiation. *Nature* **518**, 344–9 (2015).
- 979 104. Boulay, G. *et al.* OTX2 activity at distal regulatory elements shapes the
980 chromatin landscape of group 3 medulloblastoma. *Cancer Discov.* **7**, 288–301
981 (2017).
- 982 105. Budry, L. *et al.* The selector gene Pax7 dictates alternate pituitary cell fates
983 through its pioneer action on chromatin remodeling. *Genes Dev.* **26**, 2299–
984 2310 (2012).
- 985 106. Mayran, A. *et al.* Pioneer factor Pax7 deploys a stable enhancer repertoire for
986 specification of cell fate. *Nat. Genet.* **50**, 259–269 (2018).
- 987 107. McKinnell, I. W. *et al.* Pax7 activates myogenic genes by recruitment of a
988 histone methyltransferase complex. *Nat. Cell Biol.* **10**, 77–84 (2008).
- 989 108. Adam, R. C. *et al.* Pioneer factors govern super-enhancer dynamics in stem
990 cell plasticity and lineage choice. *Nature* **521**, 366–70 (2015).
- 991 109. Gaston, K. & Fried, M. CpG methylation has differential effects on the binding
992 of YY1 and ETS proteins to the bi-directional promoter of the Surf-1 and surf-2
993 genes. *Nucleic Acids Res.* **23**, 901–909 (1995).
- 994 110. Cirillo, L. A. *et al.* Binding of the winged-helix transcription factor HNF3 to a
995 linker histone site on the nucleosome. *EMBO J.* **17**, 244–254 (1998).

- 996 111. Donaghey, J. *et al.* Genetic determinants and epigenetic effects of pioneer-
997 factor occupancy. *Nat. Genet.* **50**, 250–258 (2018).
- 998 112. Lukoseviciute, M. *et al.* From pioneer to repressor: bimodal FOXD3 activity
999 dynamically remodels neural crest regulatory landscape in vivo. *Dev. Cell* **47**,
1000 608-628.e6 (2018).
- 1001 113. Kovesdi, I., Reichel, R. & Nevins, J. R. Role of an adenovirus E2 promoter
1002 binding factor in E1A-mediated coordinate gene control. *Proc. Natl. Acad. Sci.*
1003 **84**, 2180–2184 (1987).
- 1004 114. Campanero, M. R., Armstrong, M. I. & Flemington, E. K. CpG methylation as a
1005 mechanism for the regulation of E2F activity. *Proc. Natl. Acad. Sci.* **97**, 6481–
1006 6486 (2000).
- 1007 115. Wolffe, A. P. *et al.* DNMT1 forms a complex with Rb, E2F1 and HDAC1 and
1008 represses transcription from E2F-responsive promoters. *Nat. Genet.* **25**, 338–
1009 342 (2000).
- 1010 116. Perini, G., Diolaiti, D., Porro, A. & Della Valle, G. In vivo transcriptional
1011 regulation of N-Myc target genes is controlled by E-box methylation. *Proc.*
1012 *Natl. Acad. Sci.* **102**, 12117–12122 (2005).

1013

1014 **Figure Legends**

1015 **Figure 1. Validation of the experimental approach (Hi-TransMet) to test for TF**
1016 **effect on DNA methylation.**

1017 (a) Schematic representation of Hi-TransMet. PF motifs flanked by unique barcode
1018 sequences were individually cloned at the center of an intermediate-CpG content
1019 bacterial DNA fragment (FR1) within an RMCE donor plasmid. Motif-containing
1020 plasmid libraries were transfected into mESCs following *in vitro* methylation via
1021 M.SssI enzyme (+SssI) or without further treatment (–SssI). Insertion of the –SssI
1022 library results in *de novo* methylation. Methylation levels in cells that underwent
1023 successful recombination were analyzed using universal bisulfite PCR primers
1024 designed around the inserted motifs (blue and green arrows). (b) Results allow to
1025 classify the screened PFs essentially in three classes: I) PFs that cannot bind
1026 methylated DNA or induce changes in DNA methylation; II) PFs that are able to bind
1027 unmethylated DNA and protect it from methylation; III) PFs that are able to bind
1028 methylated DNA and induce DNA demethylation. (c) Validation of the experimental
1029 approach by Bisulfite Sanger Sequencing in cell lines containing FR1 with CTCF-
1030 motifs only. Upon insertion, in the –SssI condition, FR1 undergoes *de novo*
1031 methylation. Lower methylation is observed in the presence of the CTCF WT but not
1032 Sc motif. In the +SssI condition, high levels of DNA methylation were retained by
1033 FR1 in the absence of the motif and in the presence of the CTCF Sc motif. In the
1034 presence of the CTCF WT motif, a reduction of DNA methylation levels is observed.
1035 Vertical bars correspond to CpG positions, and the color code corresponds to the
1036 percentage of methylation calculated for each CpG with a minimum coverage of 10
1037 bisulfite reads. (d) CTCF binding in the FR1 was verified by ChIP.

1038 **Figure 2. Identification of protective pioneer factors (PPFs)**

1039 (a) Heatmaps indicating methylation percentages of individual CpGs in the FR1
1040 containing WT (left panel) and Sc (right panel) motifs in the –Sssl condition. Each
1041 line represents a fragment containing the indicated motif. Each square within the line
1042 corresponds to one CpG. The methylation percentage of individual CpGs is
1043 represented in a color-code. CpGs' distance from the 5' end of the motifs is indicated
1044 below the heatmaps. CpGs in the motif, when present, are indicated as m1, m2 and
1045 m3. (b) Differential methylation between WT and Sc motifs in the FR1/–Sssl
1046 condition. Differential methylation was calculated for each CpG as $\Delta\text{met} = \% \text{met}_{\text{WT}} - \% \text{met}_{\text{Sc}}$
1047 and represented in a color-code. Results were hierarchically
1048 clustered using the complete linkage method with Euclidian distance. CpGs' distance
1049 from the 5' end of the motifs is indicated below the heatmaps. The coordinates of
1050 statistically significant hypomethylated regions (HMRs) in WT condition are indicated
1051 on the side. (c) RNA-Seq density plot of expression levels of the tested PFs in
1052 mESCs. A cut-off of $\text{Log}_2(1+\text{RPKM}) < 1$ (dashed line) was used to separate PF
1053 expression levels into low (red) and high (blue).

1054 **Figure 3. Identification of super pioneer transcription factors (SPFs)**

1055 (a) Heatmaps indicating methylation percentages of individual CpGs in the FR1
1056 containing WT (left panel) and Sc (right panel) motifs in the +Sssl condition. Each
1057 line represents a fragment containing the indicated motif. Each square within the line
1058 corresponds to one CpG. The methylation percentage of individual CpGs is
1059 represented in a color-code. CpGs' distance from the 5' end of the motifs is indicated
1060 below the heatmaps. CpGs in the motif, when present, are indicated as m1, m2 and
1061 m3. (b) Differential methylation between WT and Sc motifs in the FR1/+Sssl

1062 condition. Differential methylation was calculated for each CpG as $\Delta\text{met} = \%$
1063 $\text{met_WT} - \%$ met_Sc and represented in a color-code. Results were hierarchically
1064 clustered using the complete linkage method with Euclidian distance. CpGs' distance
1065 from the 5' end of the motifs is indicated below the heatmaps. The coordinates of
1066 statistically significant hypomethylated regions (HMRs) in WT condition are indicated
1067 on the side.

1068 **Figure 4. PPFs and SPFs are cell-type specific.**

1069 (a) Scatter plot showing differential gene expression between ESCs (x axis) and NPs
1070 (y axis) based on RNA-Seq data. Tested PFs are labeled in red. A cut-off of
1071 $\text{Log}_2(1+\text{RPKM}) < 1$ (dashed lines) was used to separate PF expression levels into low
1072 and high. (b) Volcano plot highlighting genes with a significantly different expression
1073 levels between ESCs and NPs. Cut-off indicated by the dashed lines. (c,d) Scatter
1074 plots comparing differential expression of each tested PF in ESCs and NPs against
1075 the difference in Δmet between ESCs and NPs ($\Delta\Delta\text{met} = \Delta\text{met_ESCs} - \Delta\text{met_NPs}$)
1076 of the FR1 containing the corresponding PF motif in -Sssl (c) and +Sssl (d)
1077 conditions. Each dot represents changes in average Δmet of FR1 fragment with one
1078 motif. r = Pearson correlation coefficient; p = p-value. (e,f) Differential methylation
1079 (Δmet) between WT and Sc motifs in the FR1/-Sssl (e) and in the FR1/+Sssl (f)
1080 conditions in NPs. Differential methylation was calculated for each CpG as $\Delta\text{met} =$
1081 $\%$ $\text{met_WT} - \%$ met_Sc and represented in a color-code. Results were hierarchically
1082 clustered using the complete linkage method with Euclidian distance (see materials
1083 and methods). CpGs' distance from the 5' end of the motifs is indicated below the
1084 heatmaps. The coordinates of statistically significant hypomethylated regions
1085 (HMRs) in WT condition are indicated on the side. (g) Table summarizing identified

1086 PPFs and SPFs in ESCs and NPs.

1087 **Figure 5. Most SPFs induce TET-dependent active DNA demethylation.**

1088 (a) Heatmaps indicating methylation percentages of individual CpGs in the FR1
1089 containing WT (left panel) and Sc (right panel) motifs in the +Sssl condition in TET
1090 TKO ESCs, as in figures 2a and 3a. (b) Differential methylation between WT and Sc
1091 motifs in the FR1/+Sssl condition in TET TKO ESCs, as in previous figures. (c)
1092 Scatter plot showing differential gene expression between WT (x axis) and TET TKO
1093 (y axis) ESCs based on RNA-Seq data. Tested PFs as well as TET genes are
1094 labeled in red. A cut-off of $\text{Log}_2(1+\text{RPKM}) > 1$ (dashed lines) was used to separate
1095 PF expression levels into low and high.

1096 **Figure 6. SOX2 inhibits DNMT1-dependent maintenance of DNA methylation**
1097 **during replication.**

1098 (a) *In vitro* methylation assay to measure DNMT1-mediated DNA methylation using
1099 hemi-methylated probes containing WT or Sc PF motifs in the presence or absence
1100 of the corresponding PF. Relative DNMT1 activity is represented as scintillation
1101 counts, corrected for the weight of isolated DNA probes and compared to the Sc
1102 probe. Results are shown as mean + SEM of three biological triplicates. SOX2, ETS
1103 and OTX2 significantly reduce DNMT1 activity (ETS1 $p = 0.0018$, OTX2 $p = 0.0238$,
1104 SOX2 $p = 0.026$, two-tailed unpaired t-test). (b) *In vitro* methylation assay using the
1105 OCT4-SOX2 motifs in the presence of SOX2 alone, SOX2+OCT4 and OCT4 alone.
1106 Results are shown as mean + SEM of three biological triplicates (SOX2+OCT4 $p =$
1107 0.0035 , SOX2 $p = 0.0185$, two-tailed unpaired t-test). (c) *In vitro* replication assay to
1108 assess the effect of TF binding on the maintenance of DNA methylation during
1109 replication. Methylation levels following replication are measured based on the

1110 integration of radioactively labeled methyl group during replication. Results are
1111 presented as mean \pm SD of five biological replicates and analyzed as radioactive
1112 signal in the presence of SOX2 relative to the signal in absence of SOX2. P values:
1113 SOX2_WT 370nM p=0.1026, 555nM p=0.0004; SOX2_Sc 370nM p=0.4521,
1114 555nM=0.0491, two-tailed unpaired t-test. **d)** Bisulfite Sanger sequencing analysis of
1115 a bacterial DNA fragment before or after replication (\pm T-Ag) and in the absence or
1116 presence of the PF (\pm PF). Vertical bars correspond to CpG positions, and the color
1117 code corresponds to the percentage of methylation calculated for each CpG with a
1118 minimum coverage of 10 bisulfite reads.

1119 **Figure 7. Hierarchy of Transcription Factor binding.**

1120 **(a)** super pioneer transcription factors (SPFs) engage their target sequences in
1121 closed chromatin and in the presence of DNA methylation. Upon binding, most SPFs
1122 drive DNA demethylation through active processes, mainly mediated by the TET
1123 enzymes, whereas SOX2 leads to passive DNA demethylation. Loss of DNA
1124 methylation allows the binding of methylation sensitive PFs. Nucleosome
1125 remodelling and deposition of histone modifications associated with open chromatin
1126 regions, mediated by both SPFs and PFs, create a favorable environment for the
1127 binding of “settler” TFs.

1128 **Supplementary Figure 1. Experimental approach.**

1129 **(a)** Schematic representation of the Hi-TransMet approach. A library of targeting
1130 plasmids each containing the same bacterial DNA (grey line) but a different motif
1131 (colored rectangles) and barcode (dashed box) and flanked by *LoxP* sites (triangles)
1132 were transfected into ESCs containing the RMCE site together with a plasmid
1133 expressing CRE recombinase. This leads to the replacement of the selection

1134 cassette (Hygromycin/Thymidine Kinase) by the bacterial fragment. Ganciclovir
1135 treatment selects the cells that underwent recombination. Genomic DNA is extracted
1136 from successfully-recombined cells and treated with sodium bisulfite. **(b)** Sequence
1137 of the bacterial fragment FR1 used in this study. Primer sequences for Bisulfite PCR
1138 and library preparation are indicated in green. US_Primer is the upstream primer
1139 pair, DS_Primer is the downstream primer pair (please refer to text for further
1140 details). Edits to the original sequence⁴² are indicated in dark blue (additions) and
1141 light blue (changes of position). The fragment was inserted into the RMCE donor
1142 plasmid by directional cloning using the restriction enzymes BamHI and HindIII
1143 (flags); motifs were later inserted by directional cloning with SphI and NheI (flags).

1144 **Supplementary Figure 2. Hi-TransMet library preparation and molecular**
1145 **barcoding.**

1146 **(a)** NGS library preparation. Step 1, UMI assignment. A target-specific reverse
1147 primer, including of a UMI tag (colored Ns) and a library barcode (black) is annealed
1148 to the bisulfite-converted DNA and the target sequence is extended. Step 2, non-
1149 barcoded amplification. A short PCR amplification is performed using forward target-
1150 specific primers and a reverse universal primer. Step 3, addition of sequencing
1151 adapters by PCR amplification. Unused primers and primer dimers are removed
1152 between each step. The region of interest surrounding the motifs is PCR amplified
1153 using two sets of universal primers, upstream and downstream of the motifs,
1154 covering about 500 bp flanking the binding sites. **(b)** Overview of the bioinformatic
1155 pipeline.

1156 **Supplementary Figure 3. Overall methylation levels on FR1 fragment in WT**
1157 **ESCs, NPs and TET TKO ESCs**

1158 (a) Mean ratio of CpG methylation in WT ESCs, NPs and TET TKO ESCs measured
1159 at FR1 fragments containing Sc motifs. P-values (two-tailed paired t-test): NPs/-Sssl
1160 vs ESCs/-Sssl: $p < 0.0001$; NPs/+Sssl vs ESCs/+Sssl: $p = 0.0025$; TET-TKO/+Sssl vs
1161 ESCs/+Sssl: $p < 0.0001$; TET-TKO/+Sssl vs NPs/+Sssl: $p = 0.1527$. (b) Mean ratio of
1162 non CpG methylation (CHG+CHH) in WT ESCs, NPs and TET TKO ESCs measured
1163 at FR1 fragments containing Sc motifs. P-values (two-tailed paired t-test): NPs/-Sssl
1164 vs ESCs/-Sssl: $p = 0.0010$; NPs/+Sssl vs ESCs/+Sssl: $p < 0.0001$; TET-TKO/+Sssl vs
1165 ESCs/+Sssl: $p = 0.0002$; TET-TKO/+Sssl vs NPs/+Sssl: $p < 0.0001$.

1166 **Supplementary Figure 4. Differentiation into neuronal progenitors**

1167 (a, b) Heatmaps representing methylation percentages at WT and Sc motifs in the
1168 FR1/-Sssl condition (a) and FR1/+Sssl (b). (c) qPCR validation of NP differentiation
1169 by analysis of ESC-specific (Oct4, Nanog and Sox2) and NP-specific markers
1170 (FoxA1, Pax6 and Sox9) (biological triplicate).

1171 **Supplementary Figure 5. *In vitro* replication assay**

1172 (a) Schematic representation of the *in vitro* replication assay. A bacterial DNA
1173 fragment is cloned into the SV40 replication vector containing an origin of replication.
1174 The resulting plasmid is *in vitro* methylated using the Sssl methyltransferase.
1175 Plasmid is then incubated with the SPF of interest, then replication occurs in the
1176 presence of T-Antigen and cell extract. Biotinylated, replicated DNA is purified by
1177 immunoprecipitation using streptavidin beads and DpnI digestion of the non-
1178 replicated plasmid (b). (c) SPF binding to the plasmid was verified by EMSA. (d)
1179 DNA methylation is maintained during *in vitro* DNA replication. -Sssl and +Sssl
1180 plasmids were incubated in HeLa extracts in the presence of SAM[3H] and in the
1181 presence or absence of T-Ag. DNA was purified and SAM[3H] measured by

1182 scintillation counting. Graph shows CPM - background. **(e)** Bisulfite Sanger
1183 sequencing analysis of the region surrounding the binding sites in absence or
1184 presence of replication (+/- T-Ag) and the PF (+/- PF). Vertical bars correspond to
1185 CpG positions, and the color code corresponds to the percentage of methylation
1186 calculated for each CpG with a minimum coverage of 10 bisulfite reads.

1187 **Supplementary Figure 6. ChIP validation of PF binding**

1188 **(a)** Chromatin immunoprecipitation (ChIP) to validate CREB binding in ESCs and
1189 NPs. Single-motif containing ESCs were generated by RMCE insertion of
1190 FR1/CREB_WT and FR1/CREB_Sc fragments individually. Cells were then
1191 differentiated into NPs. Results are shown as mean + SEM of three biological
1192 replicates. P-values (two-tailed unpaired t-test): WT_NPs/-Sssl vs Sc_NPs/-Sssl:
1193 $p=0.0202$; WT_ESCs/-Sssl vs WT_NPs/-Sssl: $p=0.0168$; WT_ESCs/+Sssl vs
1194 WT_NPs/+Sssl: $p=0.0340$. **(b)** SOX2 ChIP in ESCs and NPs containing the OCT4-
1195 SOX2 motif. P-value WT_ESCs/+Sssl vs Sc_ESCs/+Sssl: 0.0012 (two-tailed
1196 unpaired t-test) **(c)** OCT4 ChIP in ESCs and NPs containing the OCT4-SOX2 motif.
1197 **(d)** SOX2 ChIP in SOX2-motif containing ESCs. **(e)** NRF1 ChIP in NRF1-motif
1198 containing ESCs.

1199

1200 **Tables**

1201 **Supplementary Table 1. List of PFs selected for RMCE screening. DNA binding**

1202 domains are reported as indicated in the Human TFs database

1203 (<http://humantfs.ccb.utoronto.ca/>)⁸⁷. For each factor, the main references for:

1204 pioneering activity; sensitivity or binding to methylated DNA; suspected DNA

1205 demethylation capacity and/or suspected or proven interactions with TETs and

1206 DNMTs are indicated

PF	DNA Binding Domain	Pioneering Activity	DNA methylation sensitivity	Suspected DNA demethylation capacity
CTCF	C2H2 Zinc Finger	88	Binds 5mC ^{14,38,89}	Yes ^{14,38} Interacts with TET ³⁴ Interacts with DNMT1 ³³
KAISO	C2H2 Zinc Finger	88	Binds 5mC ^{11,90,91}	
KLF4	C2H2 Zinc Finger	25,31,60,92,93	Binds 5mC ^{10,11,91}	Yes ³¹
KLF7	C2H2 Zinc Finger	88	Binds 5mC ¹⁷⁸	
REST	C2H2 Zinc Finger		Binds 5mC ¹⁴	Yes ^{14,30} Interacts with TET ³⁹⁴
ZBTB14	C2H2 Zinc Finger	88	Binds C ⁹⁰	
ER	Zinc Finger (NHR type)	95	Binds 5mC ¹¹	Yes ⁹⁶
GR	Zinc Finger (NHR type)	95		Yes ⁹⁷
GATA	Zinc Finger (GATA type)	4,98,99	Binds 5mC ^{10,100}	Yes ^{100,101}
NANOG	Homeodomain	102,103	Binds 5mC ¹⁷⁸	Yes ¹⁰³ No ¹⁰¹ Interacts with TET ³²
OTX2	Homeodomain	103,104		Yes ¹⁰³
OCT4	Homeodomain + POU	25,60,92,93	Binds 5mC ¹¹	No ¹⁰¹
PAX7	Homeodomain + Paired box	105–107	Binds 5mC ¹¹	Yes ¹⁰⁶
SOX2	HMG/SOX	25,60,64,92,93		No ¹⁰¹
SOX9	HMG/SOX	108		
SOX17	HMG/SOX			Yes ¹⁰³
ETS	ETS	88	Binds C ^{11,100,109}	

FOXA1	Forkhead (helix-turn-helix)	3,4,110	Binds 5mC ⁹⁰	Yes ^{47,111} Interacts with TET1 ⁴⁵
FOXD3	Forkhead (helix-turn-helix)	48,112		Yes ⁴⁸
CREB	Other (bZip)	88	Binds C ^{11,53,54,91}	
E2F1	Other (E2F_TDP)	88	Binds C ^{11,90,113,114} Binds 5mC ¹⁰	Interacts with DNMT1 ¹¹⁵
NFY	Other (CBF/NF-Y)	88	Binds C ¹¹	
NMYC	Other (bHLH)		Binds C ^{30,116}	No ¹⁰⁰
NRF1	Other (unknown)	88	Binds C ^{10,91} Binds 5mC ^{30,91}	No ³⁰

1207

1208 **Supplementary Table 2. List of WT and Sc PF motifs and barcodes.**

PF	Database ID	WT motif	WT barcode	Sc motif	Sc barcode
CREB	MA0018.2_CREB1	TGACGTCA	tagaga	AATCGGTC	aatgta
CTCF_1	MA0139.1_CTCF_rev	ATAGCGCCCCCTAGTGGCCA	tgagga	CCCACGGGTGGCCAACCATT	tgatga
CTCF_2	MA0139.1_CTCF	TGGCCACCAGGGGGCGCTA	tgagga	GGCAGGGAGGACCCCGTTC	tgatga
E2F1	MA0024.1_E2F1 + Chen 2008	TTTCGCGC	atgtga	TCGCTTCG	aaggag
ER	MA0112.3_ESR1	AAGGTCACGGTGACCTG	agaagt	GTA ACTCCGAGTGAGGC	aataga
ETS	MA0098.3_ETS1	ACCGGAAGTG	atgggg	GCCGAAAGTG	atggtt
FOXA1	MA0148.3_FOXA1	TCCATGTTTACTTTG	aaagtg	TATTGGTCTCTATTC	ttgtga
FOXD3	MA0041.1_Foxd3	GAATGTTTGT	tgagaa	ATTAGTTTGTGT	aagtgt
GATA	MA0482.1_Gata4	TCTTATCTCCC	agtagg	CTTCACTTCCT	tgggat
GR	MA0113.3_NR3C1	GGGTACATAATGTTCCC	atgtta	CACCTAGAAGTGTGCTT	atgtgg
KAISO	MA0527.1_ZBTB33	CTCTCGCGAGATCTG	aatatg	GTTTCGCGGACTCAC	agaggg
KLF4	MA0039.2_Klf4	TGGGCGGGGC	tgggag	GGTCCGGGGG	tatgtg
KLF7	UniProbe ID UP00093	ACGCCC	tagtgt	CCGCAC	tttga
NANOG	TRANSFAC M01123	GGGCCCATTTCC	ttaagg	CCTAGGTCCCTG	tataga
NFY	MA0060.2_NFYA	AGAGTGCTGATTGGTCCA	aaaaga	TTGGGAGTACTGGTACAC	tgtggg
NMYC	MA0104.3_Mycn	GCCACGTG	aaaaaa	CATGCGGC	tagtat
NRF1	MA0506.1_NRF1	GCGCCTGCGCA	agatat	TCGAGCCCCGGC	tgtatt
OCT4-SOX2	MA0142.1_Pou5f1:Sox2	CTTTGTTATGCAAAT	aagagt	ATACTGTGAATCTTT	tgaaag
OTX2	UniProbe ID UP00267	TTAATCCC	ttttaa	ATATCCCT	tgaaga
OCT4	MA111.5_POU5F1	ATTTGCAT	aatggt	TTTAACTG	tgtgag
PAX7	MA0680.1_PAX7	TAATCGATTA	atagga	TATACGATAT	tggata
REST	MA0138.2_REST	TTCAGCACCATGGACAGCGCC	aaaagt	CAGTTACAGCCCCCAGTCGGA	tgggaa
SOX17	MA0078.1_Sox17	TTCATTGTC	tattat	TTTCAGTCT	ttgggt
SOX2	MA0143.3_Sox2	CCTTTGTT	ttagtg	TCTGTCTT	tagaag
SOX9	Liu 2015	ACAAAGGGCCCTTTGT	ttgtta	GGCTAGTCTCATGCAA	tagata
ZBTB14	UniProbe ID UP00065	GCGCGCG	atntaa	CCGGGCG	tttgggt

1209

1210 **Supplementary Table 3. List of primers used in this study.**

Target	Purpose	Forward	Reverse
FR1 upstream	RMCE exchange	CCTCTGGGTAAATTTGGAACA	GCAGAACGCCTGAAAACTC
FR1 downstream	RMCE exchange	CACCGAAAGCAGACAAACCT	AACGCCTGAAAACTCAGGA
RMCE cassette	RMCE cassette insertion upstream	AGCAAAGGTGTTCTCATATGTCA	CAAGTGGGCAGTTTACCGTA
RMCE cassette	RMCE cassette insertion downstream	TGCACGTCTTTATCCTGGATT	GGTTTAGTCTTCTCTGTGCCT
FR1_ChIP	qPCR	ACCATGAAAGTATCAGTTCCAGGC	GTGTAAGCTCTCAACCTTAAGCA
Snrpd3	qPCR	TCTCGCCTTCGCCTTCTAAC	GGACTCTCCCGGGCAATTA
Oct4	qPCR	ATGCCGTGAAGTTGGAGAAG	GCTTGGCAAACCTGTTCTAGCT
Nanog	qPCR	TTGCTTACAAGGGTCTGCTACT	ACTGGTAGAAGAATCAGGGCT
Foxa1	qPCR	GCATGAGAGCAACGACTGG	CAGGCCGGAGTTCATGTTG
Sox9	qPCR	CAGACCAGTACCCGCATCTG	AAGGGTCTCTTCTCGCTCTC
Trkb	qPCR	GGCATTCCCGAGGTTGGA	CTGGTTTGCAATGAGAATTTCCG
Pax6	qPCR	CACCAGACTCACCTGACACC	TCACTCCGCTGTGACTGTTC
Sox2	qPCR	TAGAGCTAGACTCCGGGCGATGA	TTGCCTTAAACAAGACCACGAAA
FR1 upstream	Bisulfite PCR	AAAATTTAGGAGGTAGATAATGAGGATA	CCCCTTTAATAACAACCCAATTC
FR1 downstream	Bisulfite PCR	ATTTGAAGGGAAAGGATTAGTATGT	ACCATTAAAAAATTTTTAAACTCTTATAC

1211

1212

1213 **Supplementary Table 4. List of library barcodes.**

	Barcode	Cell line	Condition
FR1	GCGGC	TET TKO ESC	- Sssl
	TGATC	TET TKO ESC	+ Sssl
	GTGAT	WT ESC	- Sssl
	CGTGC	WT ESC	+ Sssl
	TAGCT	NP	- Sssl
	ACTGA	NP	+ Sssl

1214

1215

1216 **Supplementary Table 5. Hi-TransMet library preparation primers.**

Step	Target	Sequence
Step 1	FR1	AATGTACAGTATTGCGTTTTXXXXXNNNNNNNNCCCTTTAATAACAACCCAATTC
Step 2.	Upstream Fw	TTCTTAGCGTATTGGAGTCCAAAATTTAGGAGGTAGATAATGAGGATA
	Downstream Fw	TTCTTAGCGTATTGGAGTCCATTTGAAGGAAAGGATTAGTATGT
	Reverse	AATGTACAGTATTGCGTTTTG
Step 3	Fw with adapter	CAAGCAGAAGACGGCATACGAGATACATCGGTGACTGGAGTTCAGACGTGTGCTCTCCGATCTNNNTTCTTAGCGTATTGGAGTCC
	Rv with Adapter	AATGATACGGCGACCACCGAGATCTACACTCTTTCCTACACGACGCTCTCCGATCTGAATGTACAGTATTGCGTTTTG
		AATGATACGGCGACCACCGAGATCTACACTCTTTCCTACACGACGCTCTCCGATCTTGAATGTACAGTATTGCGTTTTG
		AATGATACGGCGACCACCGAGATCTACACTCTTTCCTACACGACGCTCTCCGATCTCTGAATGTACAGTATTGCGTTTTG
		AATGATACGGCGACCACCGAGATCTACACTCTTTCCTACACGACGCTCTCCGATCTAATGTACAGTATTGCGTTTTG

1217

1218

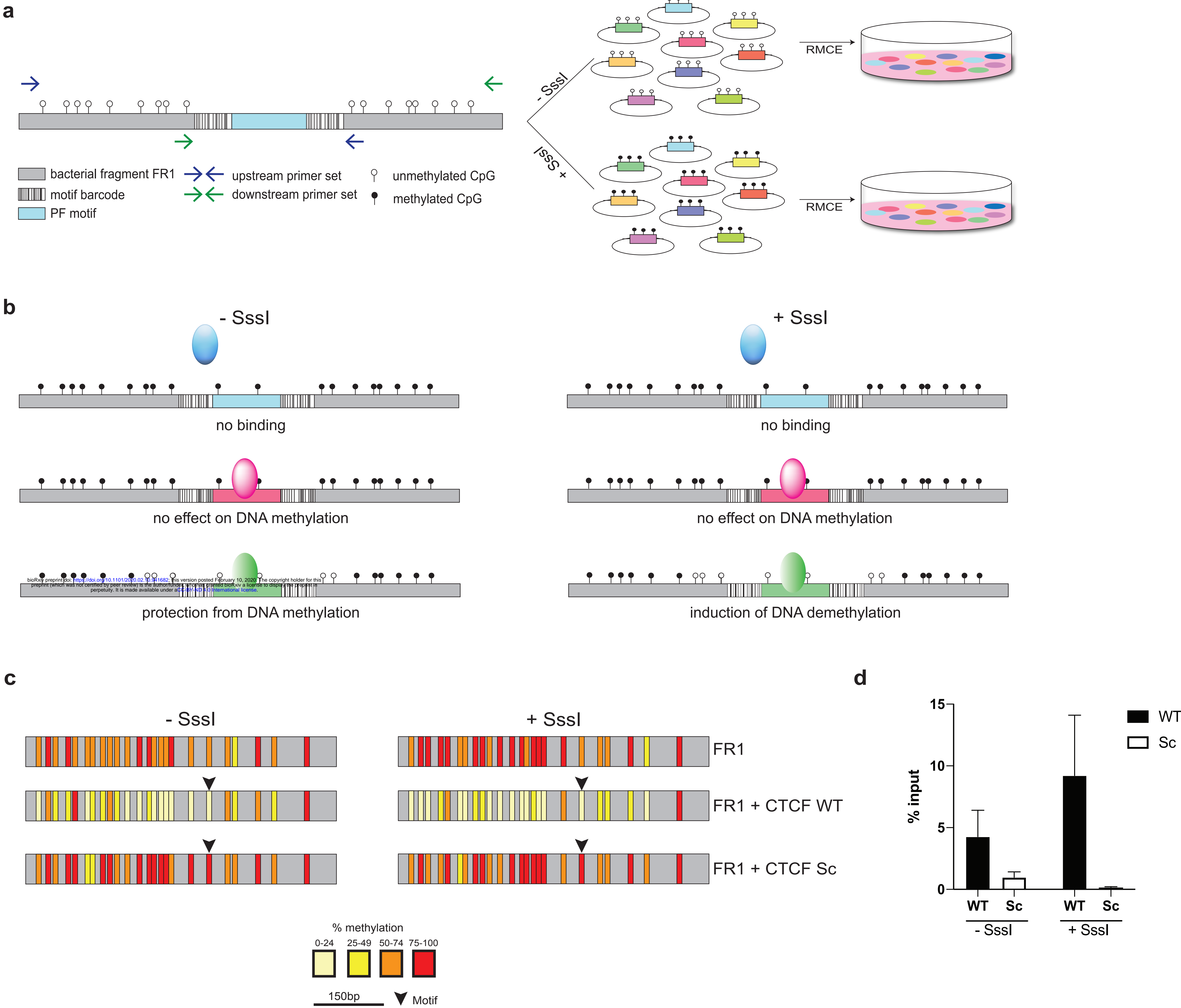
1219

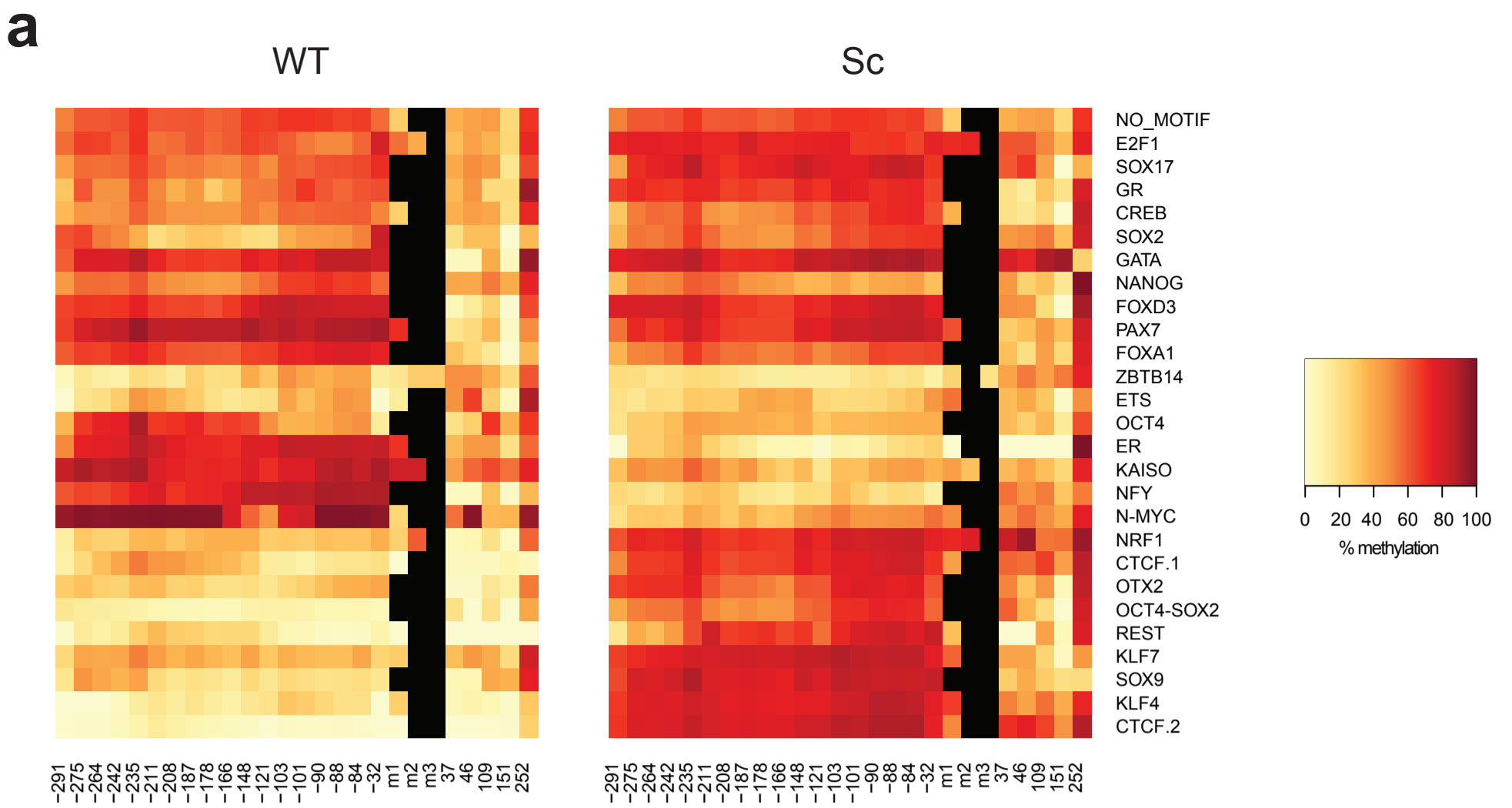
1220

1221

1222

1223





bioRxiv preprint doi: <https://doi.org/10.1101/2020.02.10.941682>; this version posted February 10, 2020. The copyright holder for this preprint (which was not certified by peer review) is the author/funder, who has granted bioRxiv a license to display the preprint in perpetuity. It is made available under aCC-BY-ND 4.0 International license.

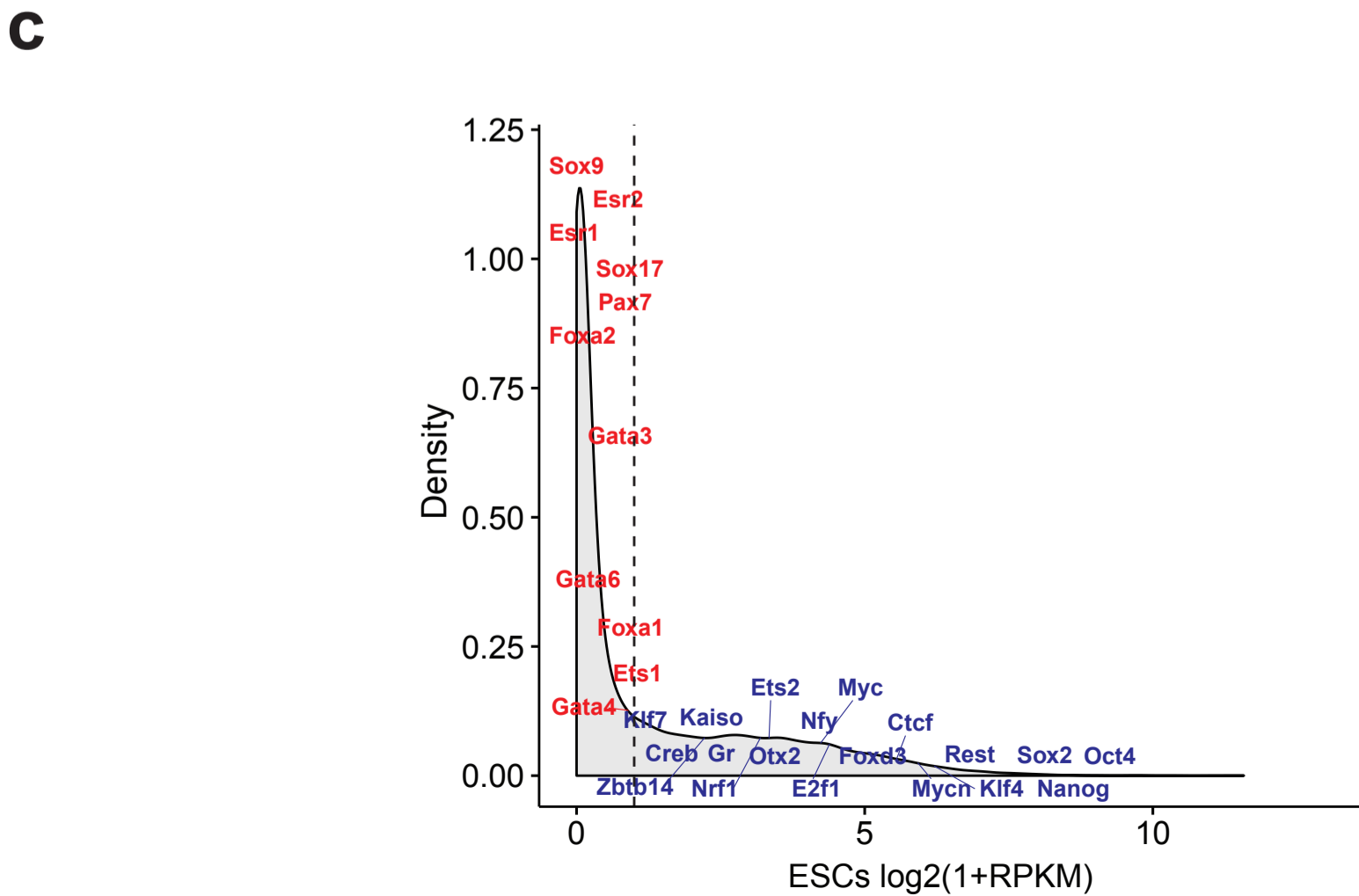
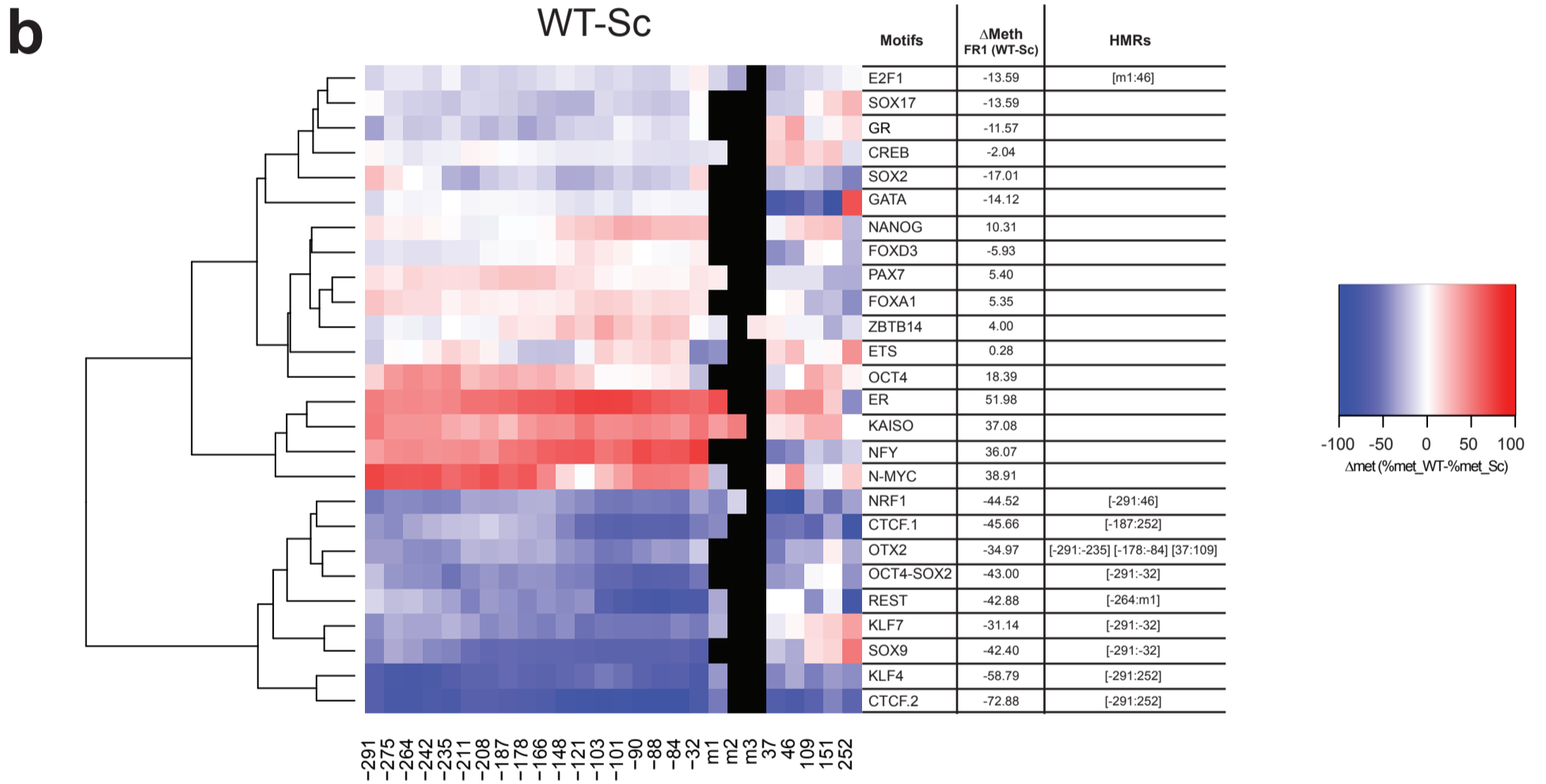
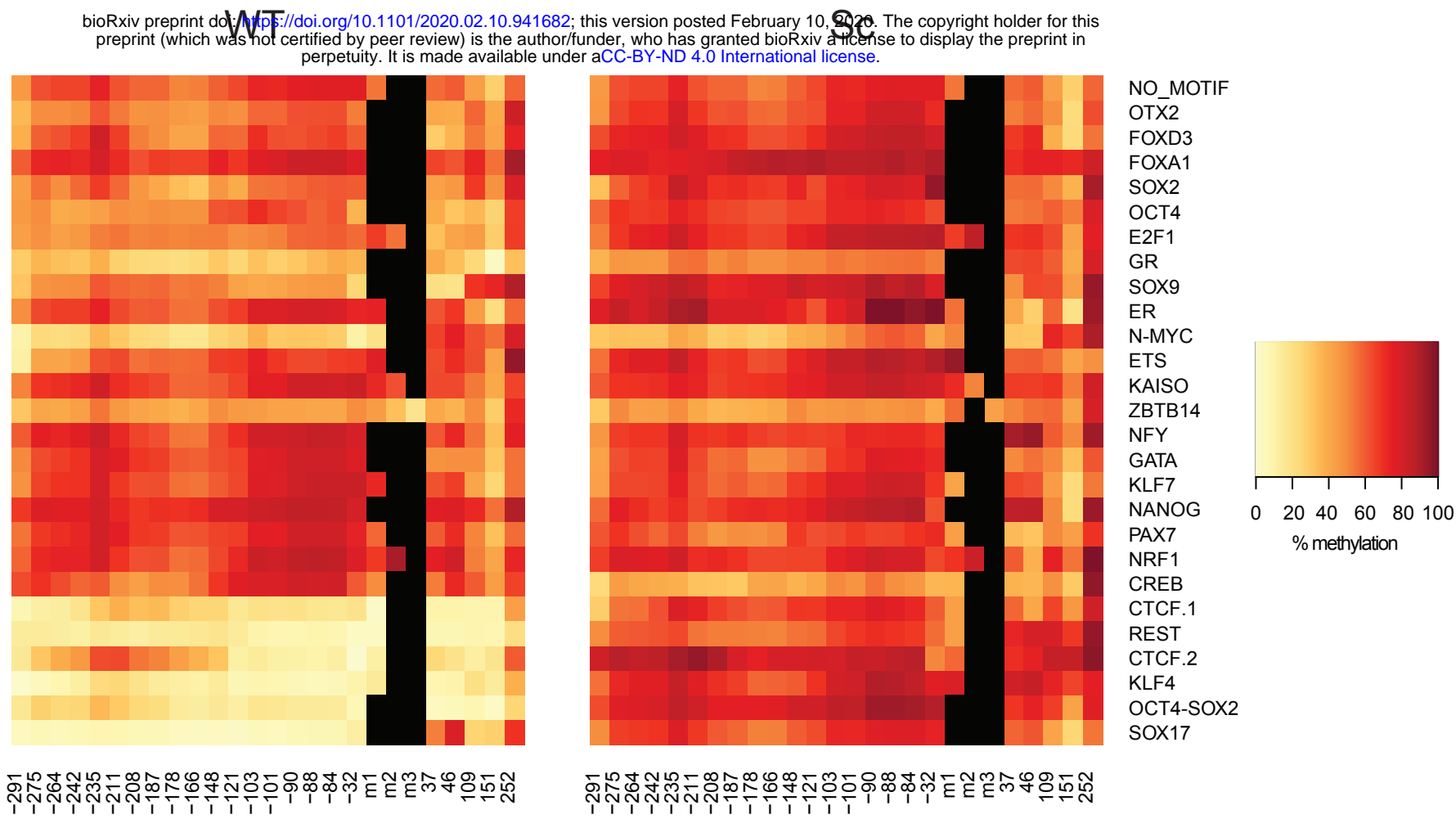


Figure 2

a



b

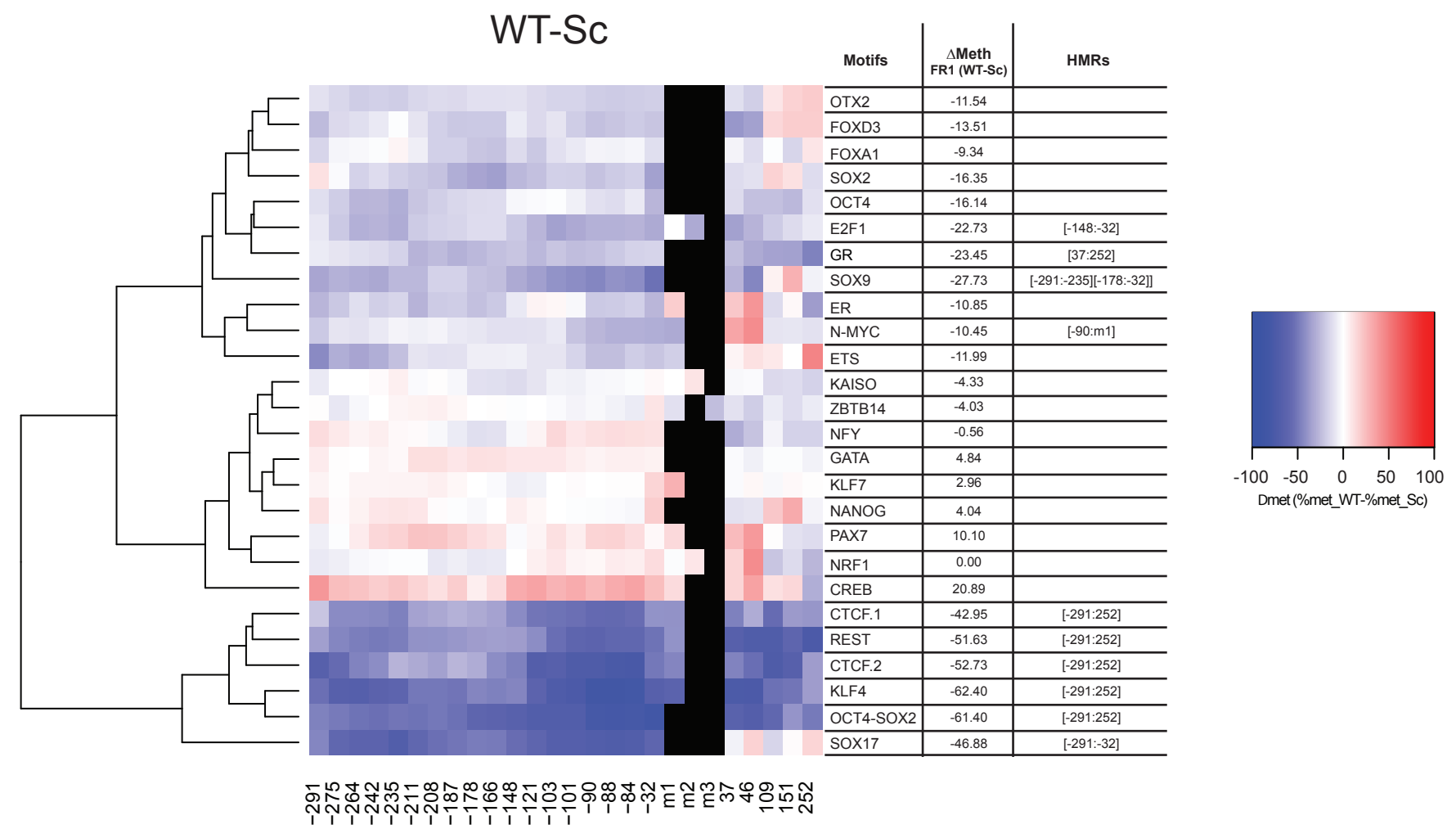
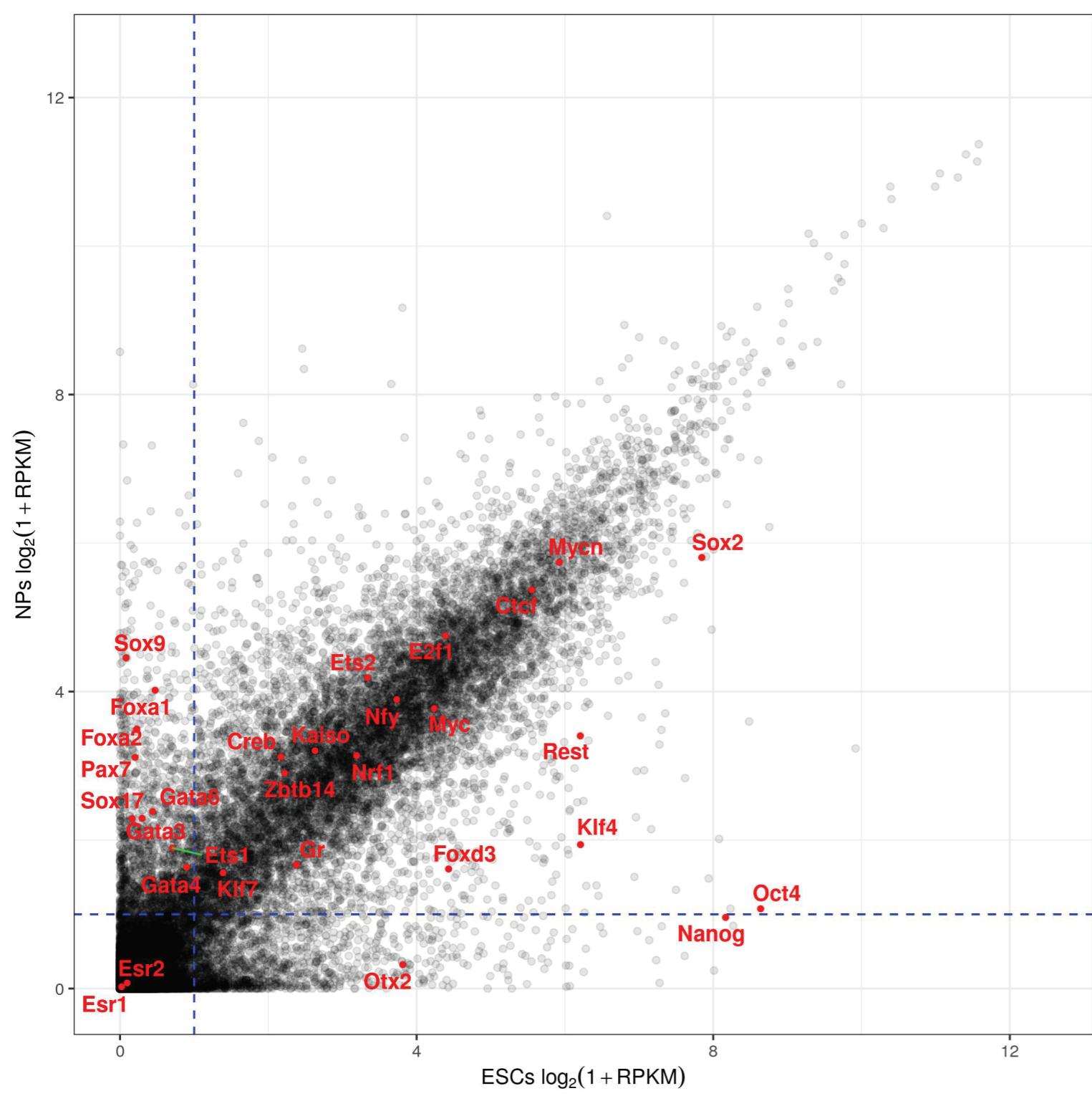
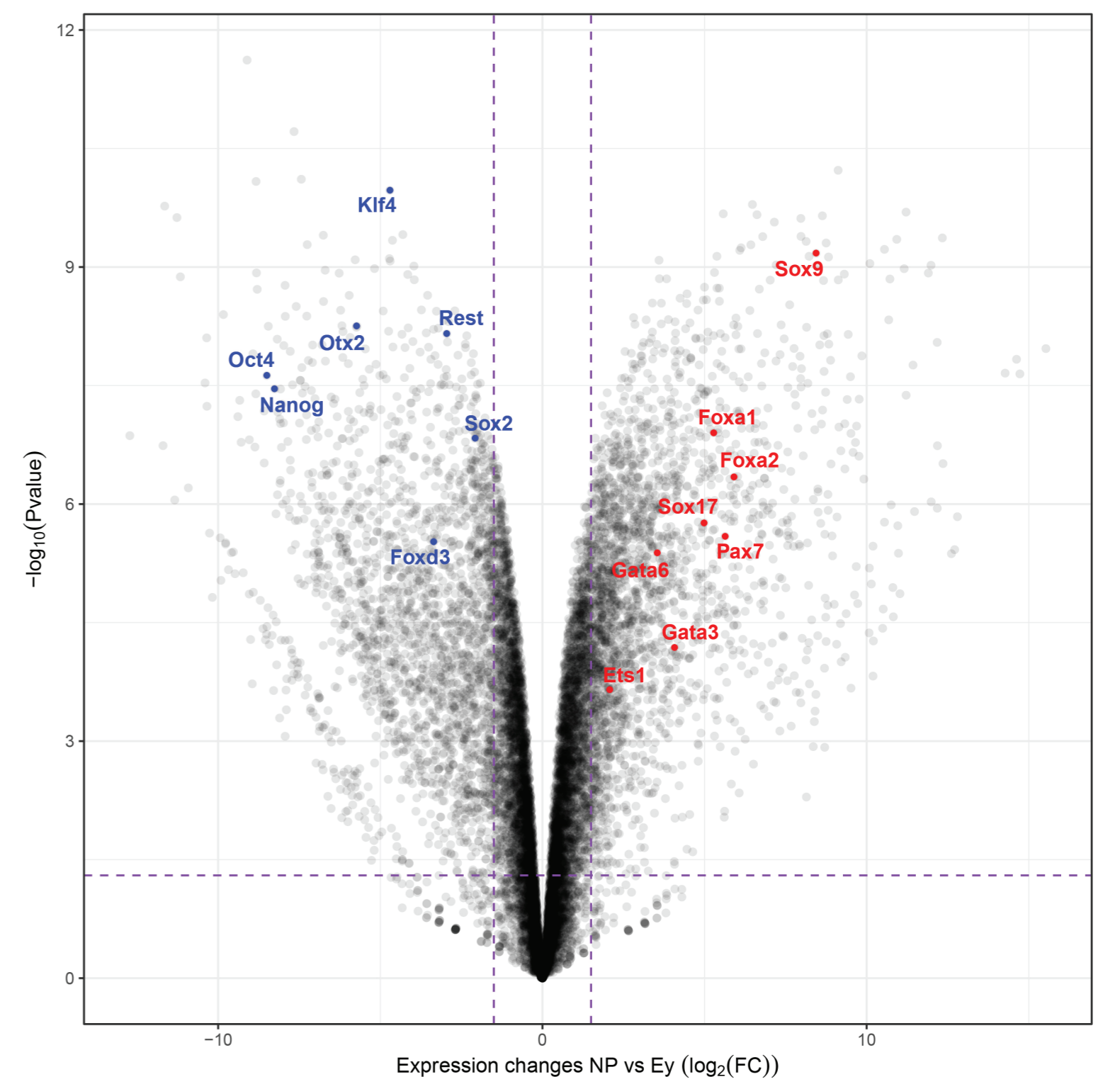


Figure 3

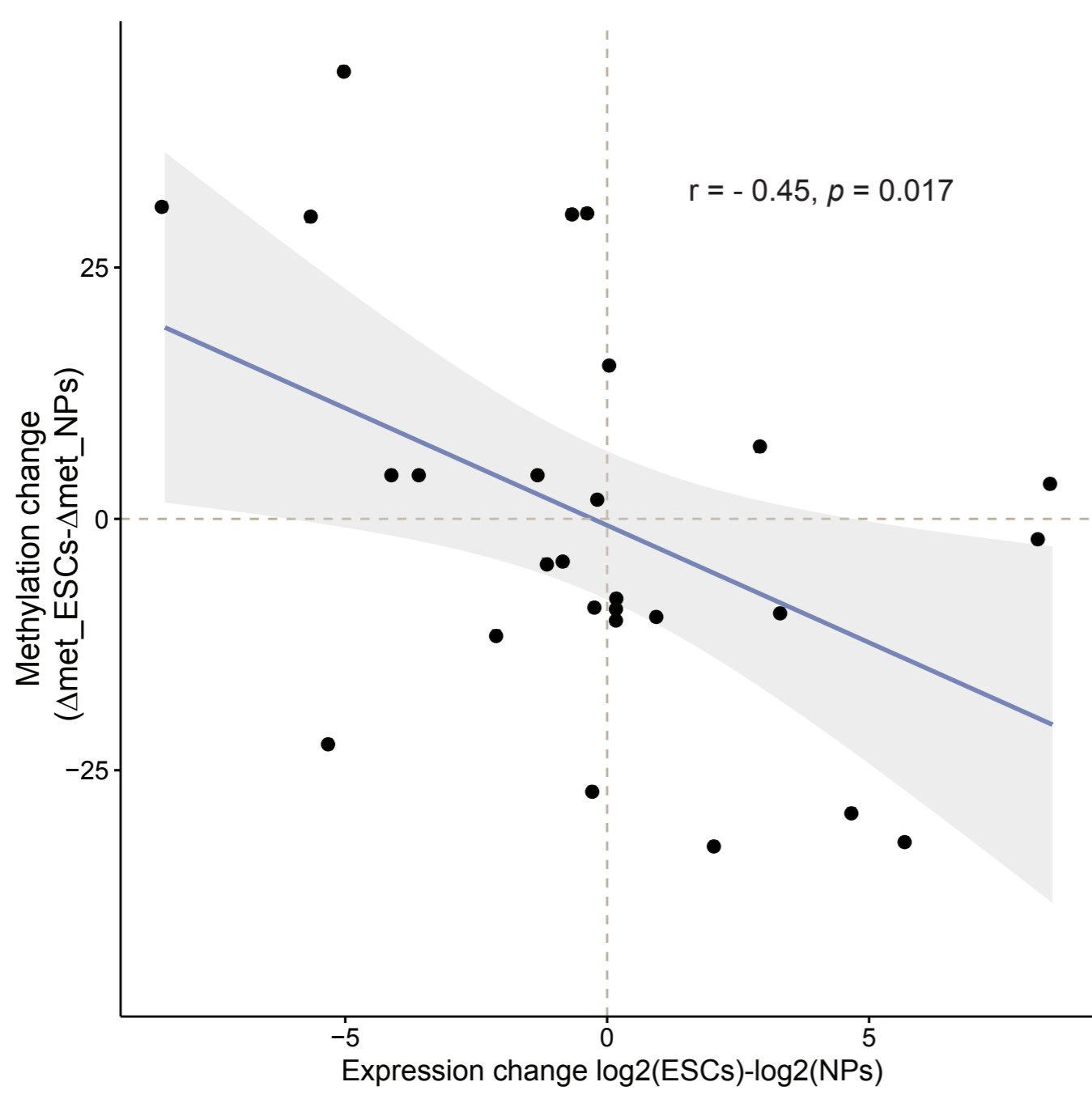
a



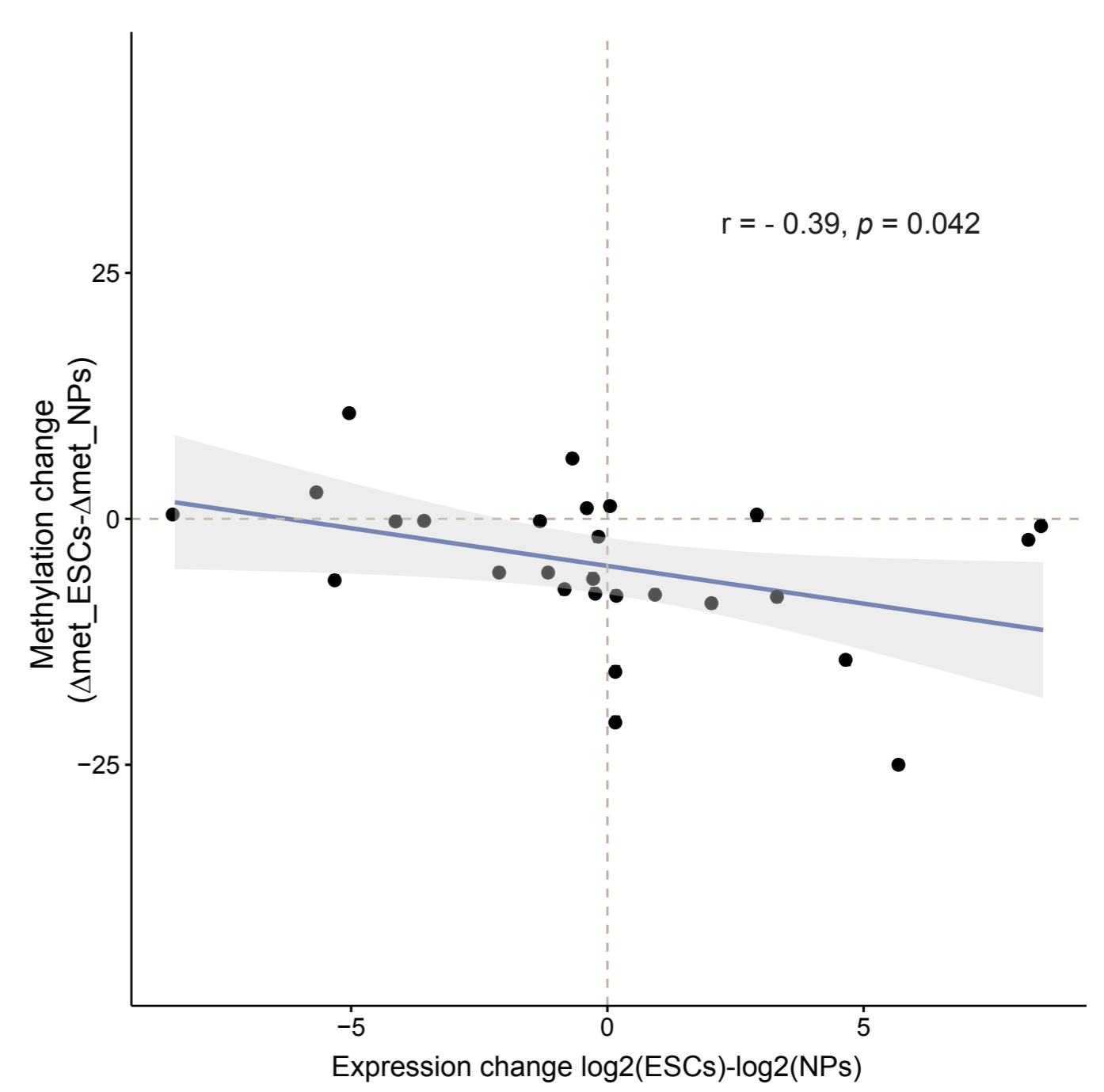
b



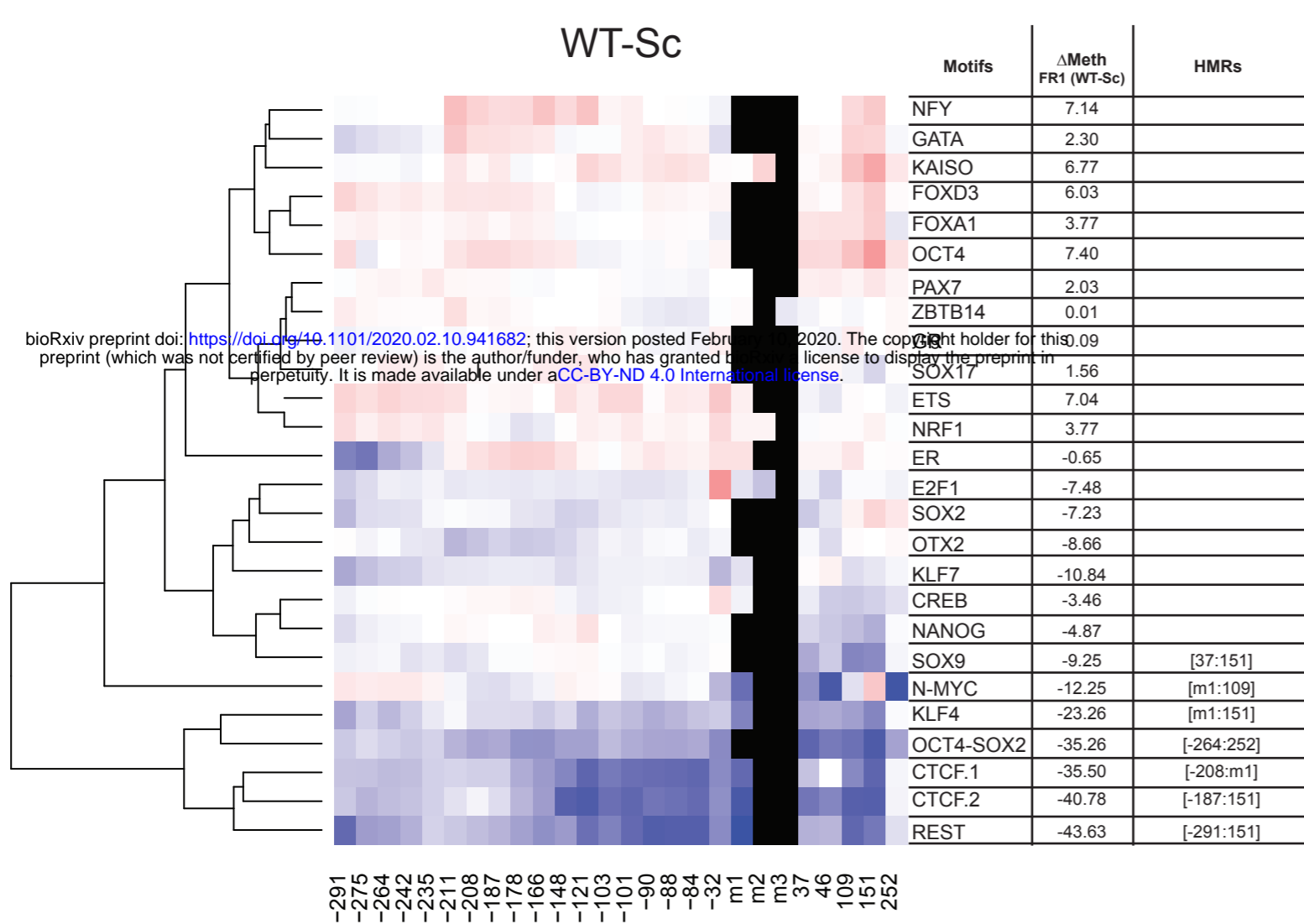
c



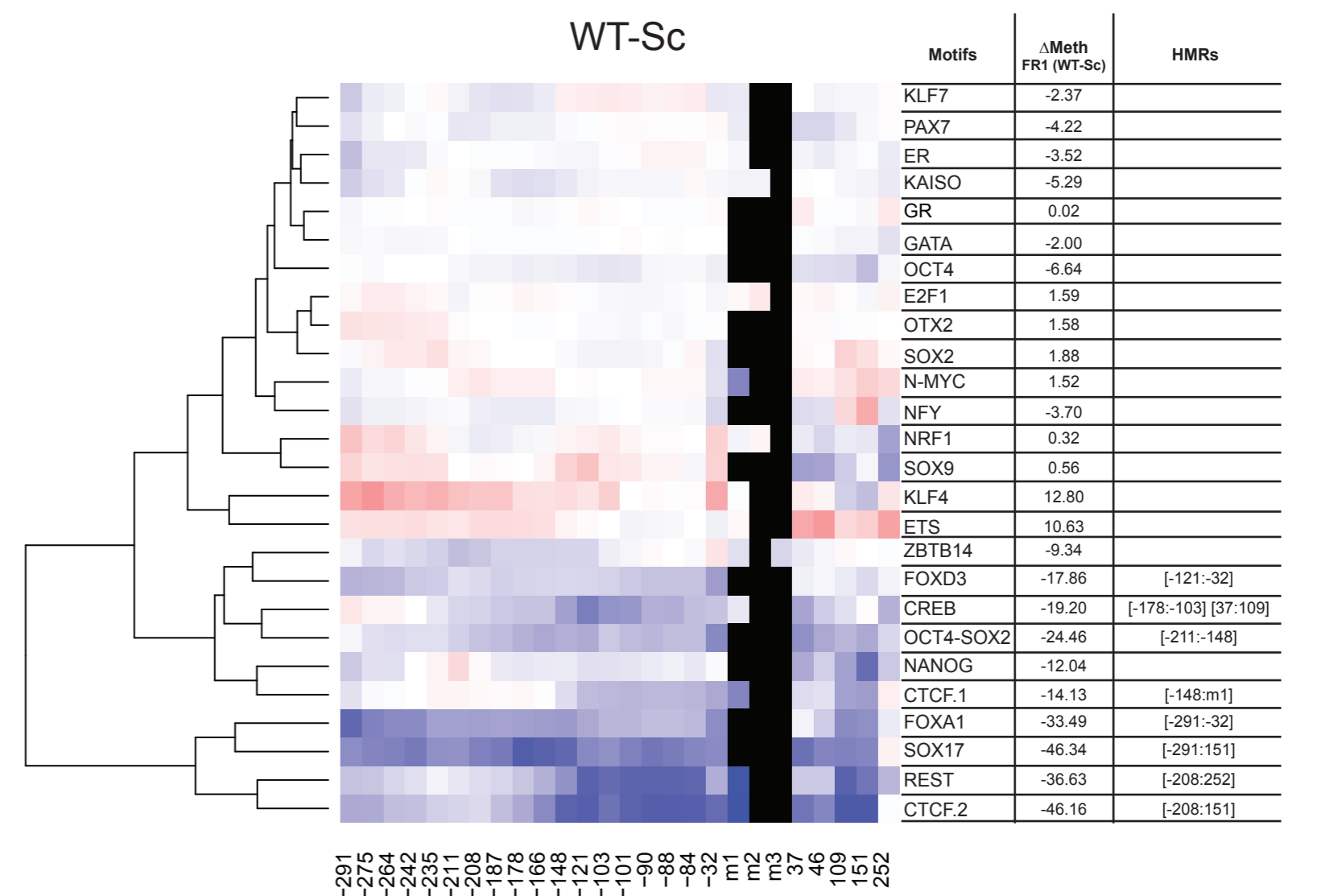
d



e

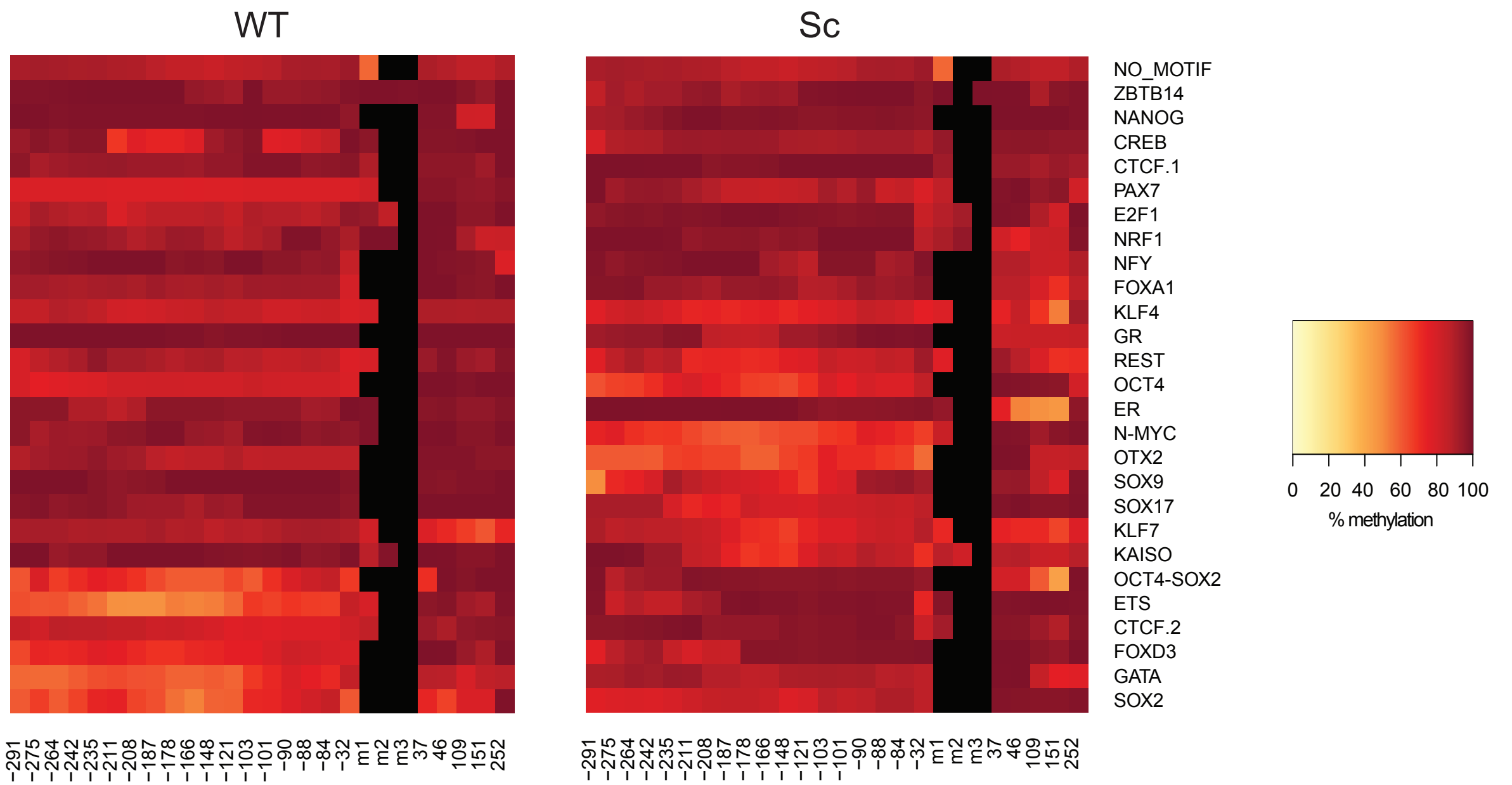


f

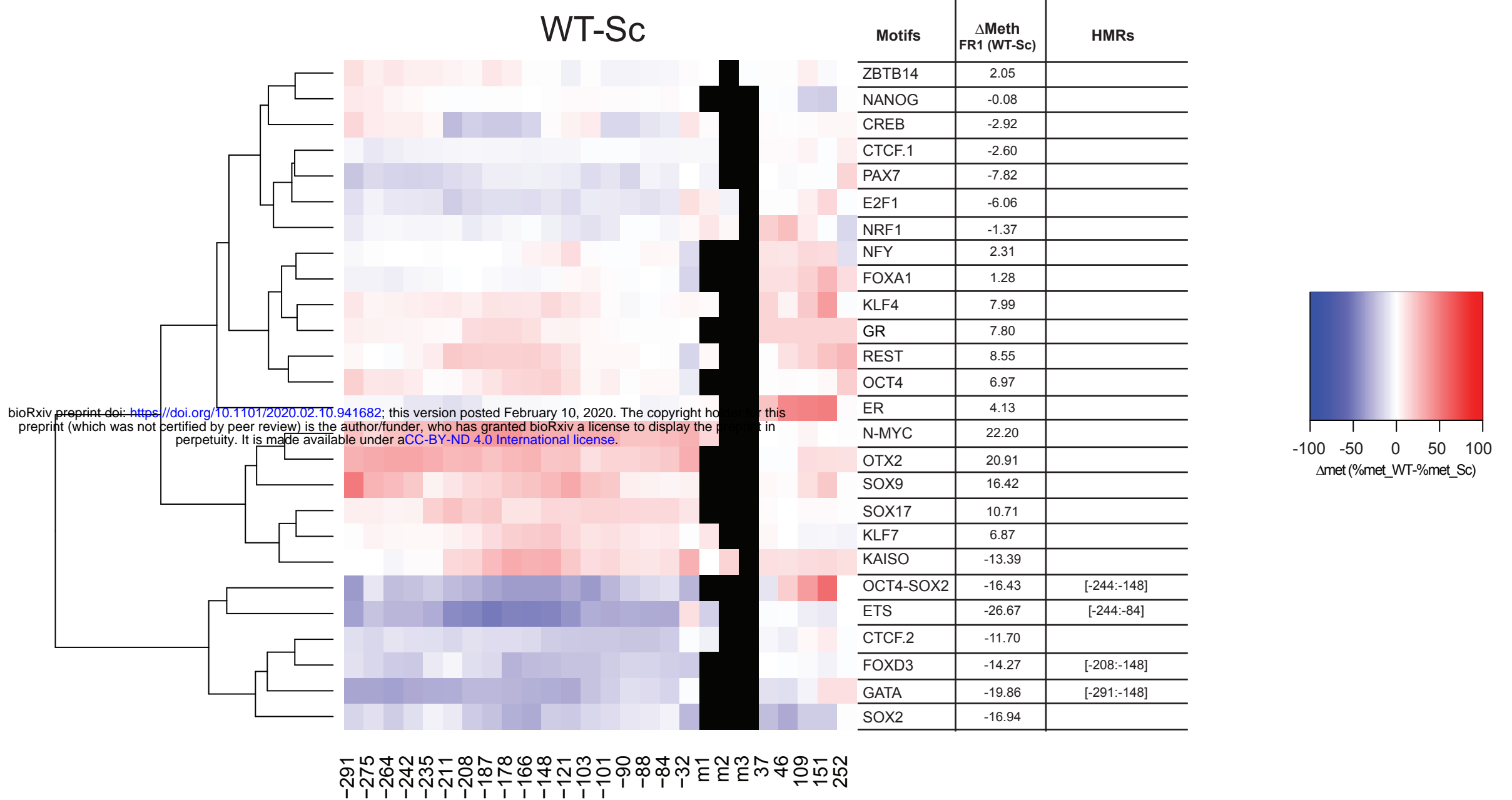


	PPFs	SPFs
ESCs	CTCF REST NRF1 KLF4 KLF7 OCT4-SOX2 E2F1 OTX2	CTCF REST KLF4 OCT4-SOX2 E2F1 N-MYC GR
NPs	CTCF REST KLF4 OCT4-SOX2 SOX9 N-MYC	CTCF REST OCT4-SOX2 SOX17 CREB FOXA1 FOXD3

a



b



c

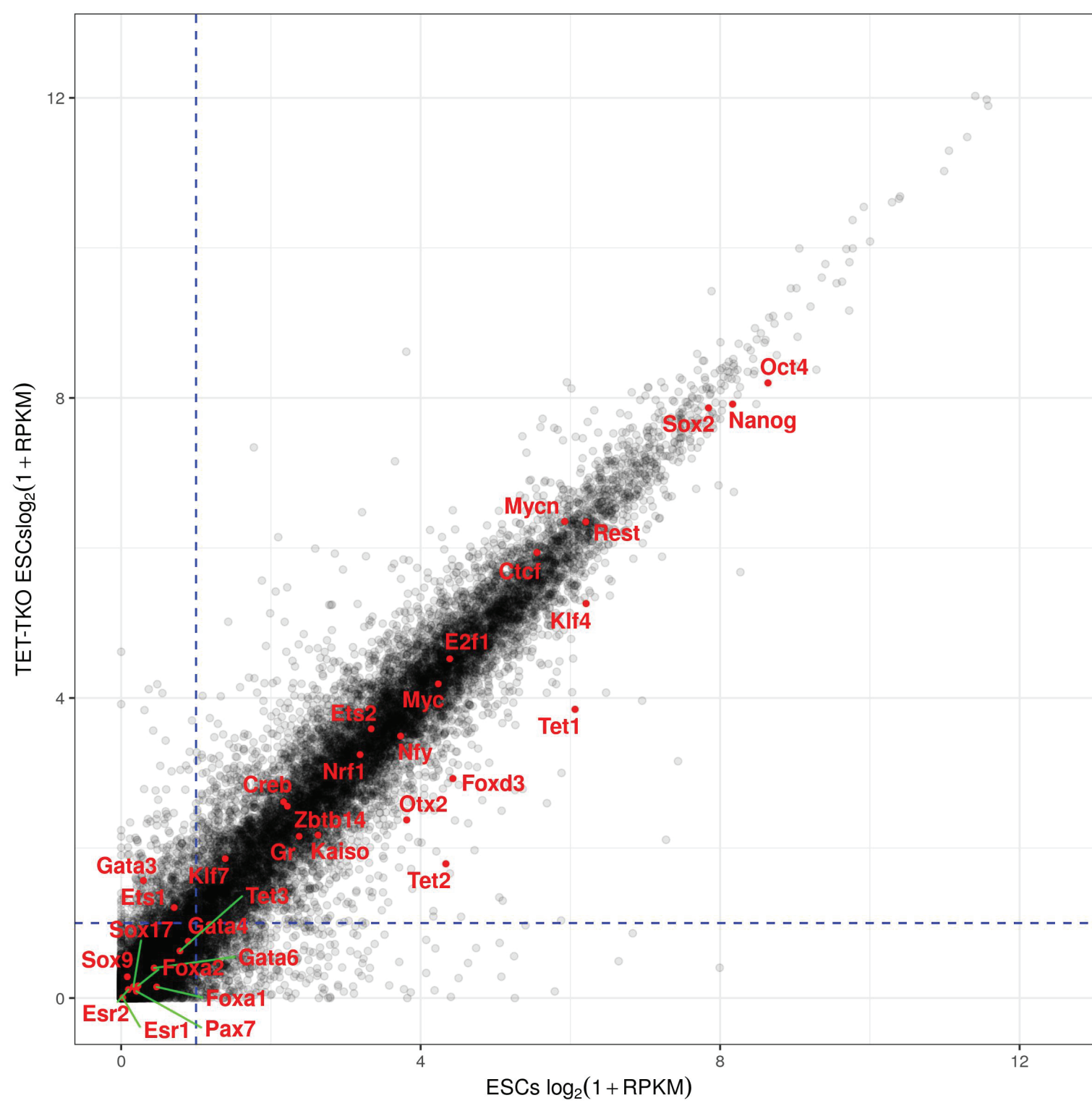


Figure 5

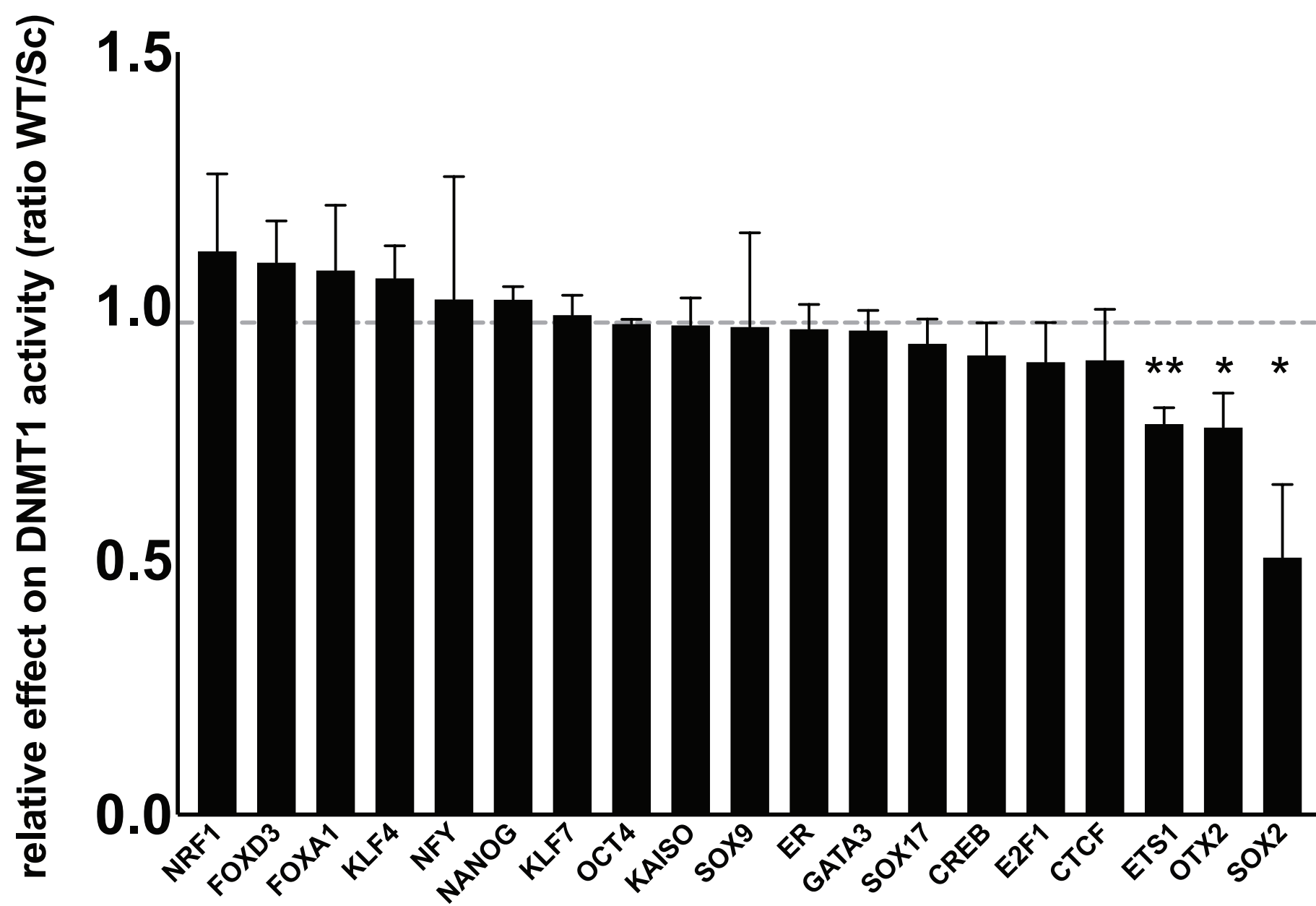
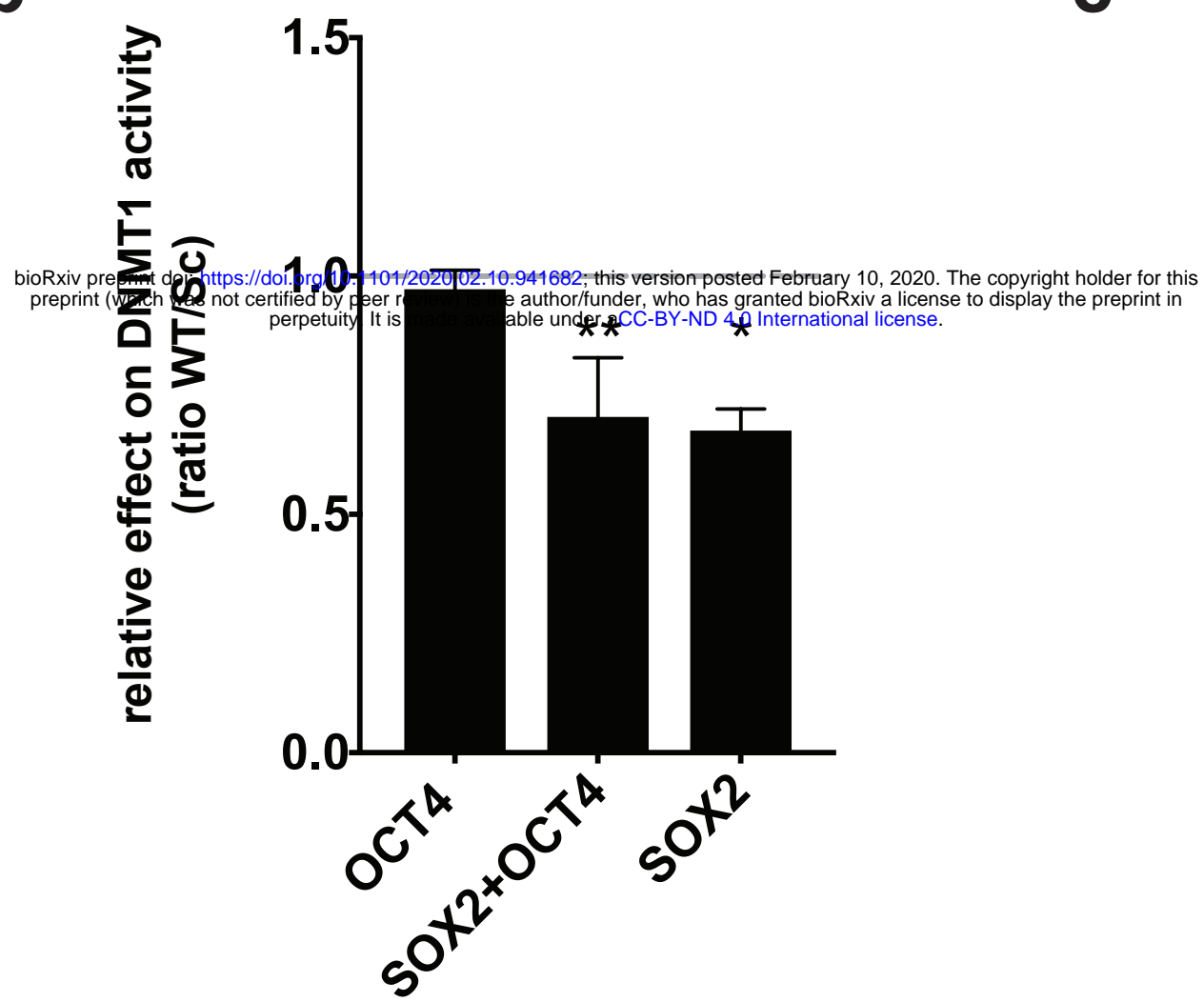
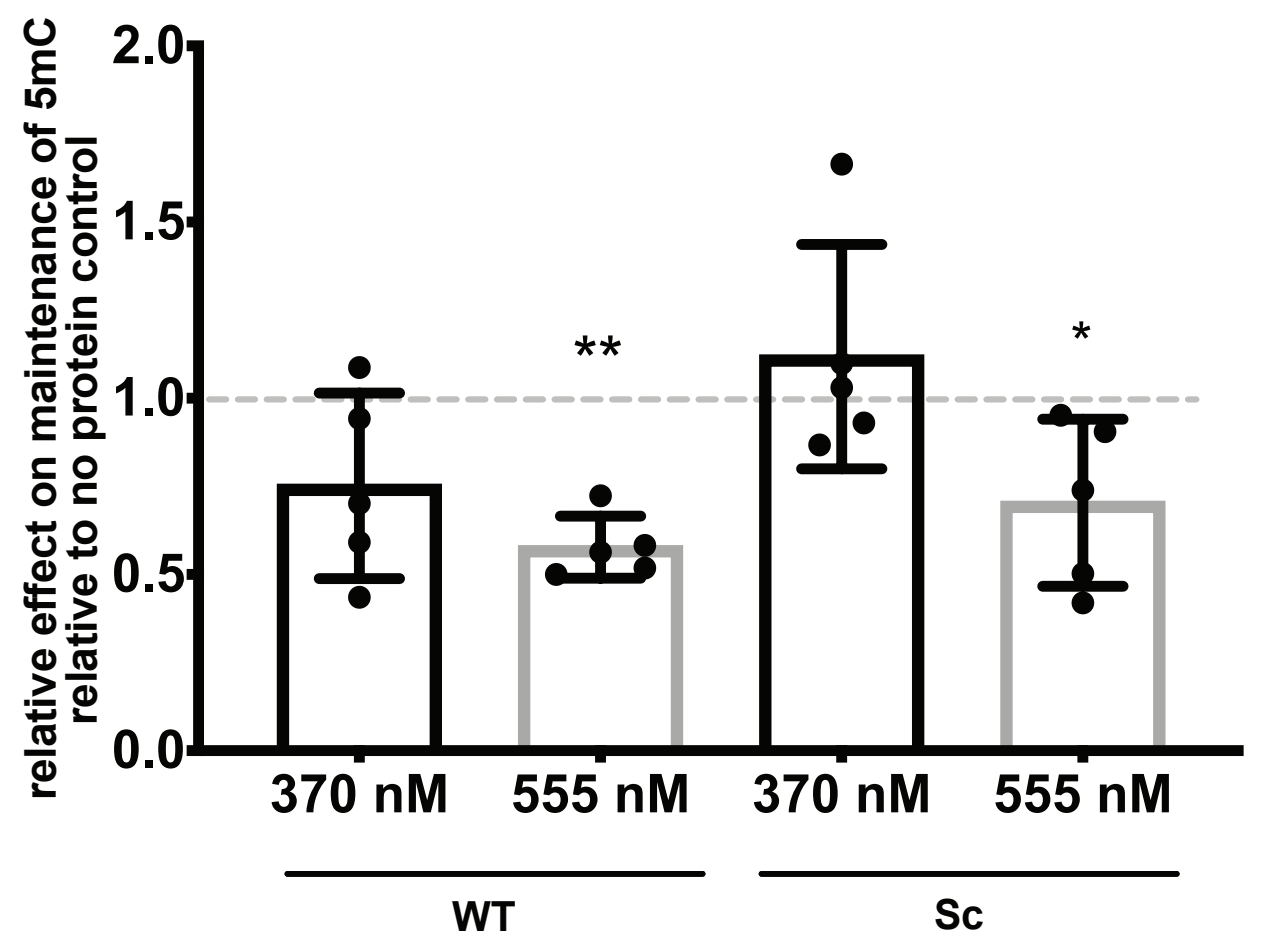
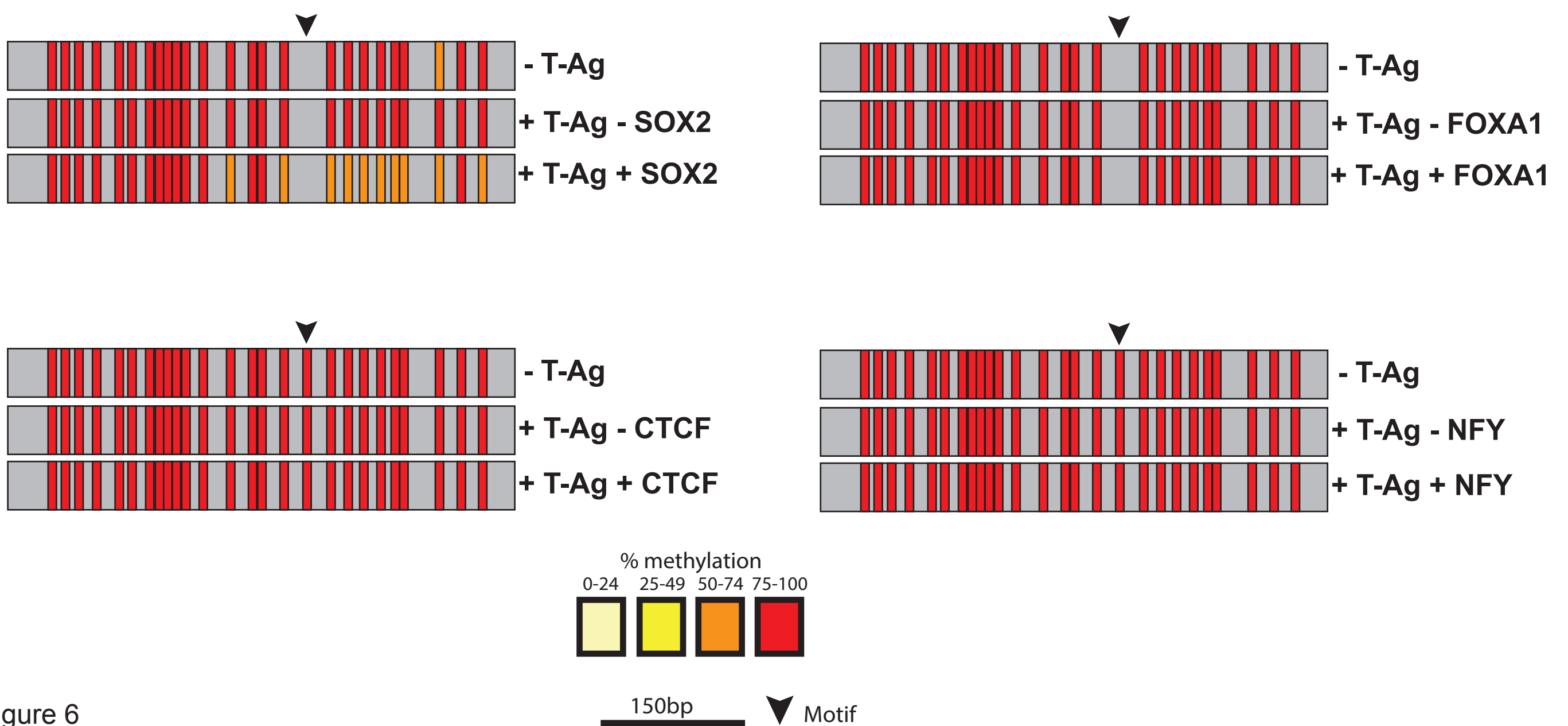
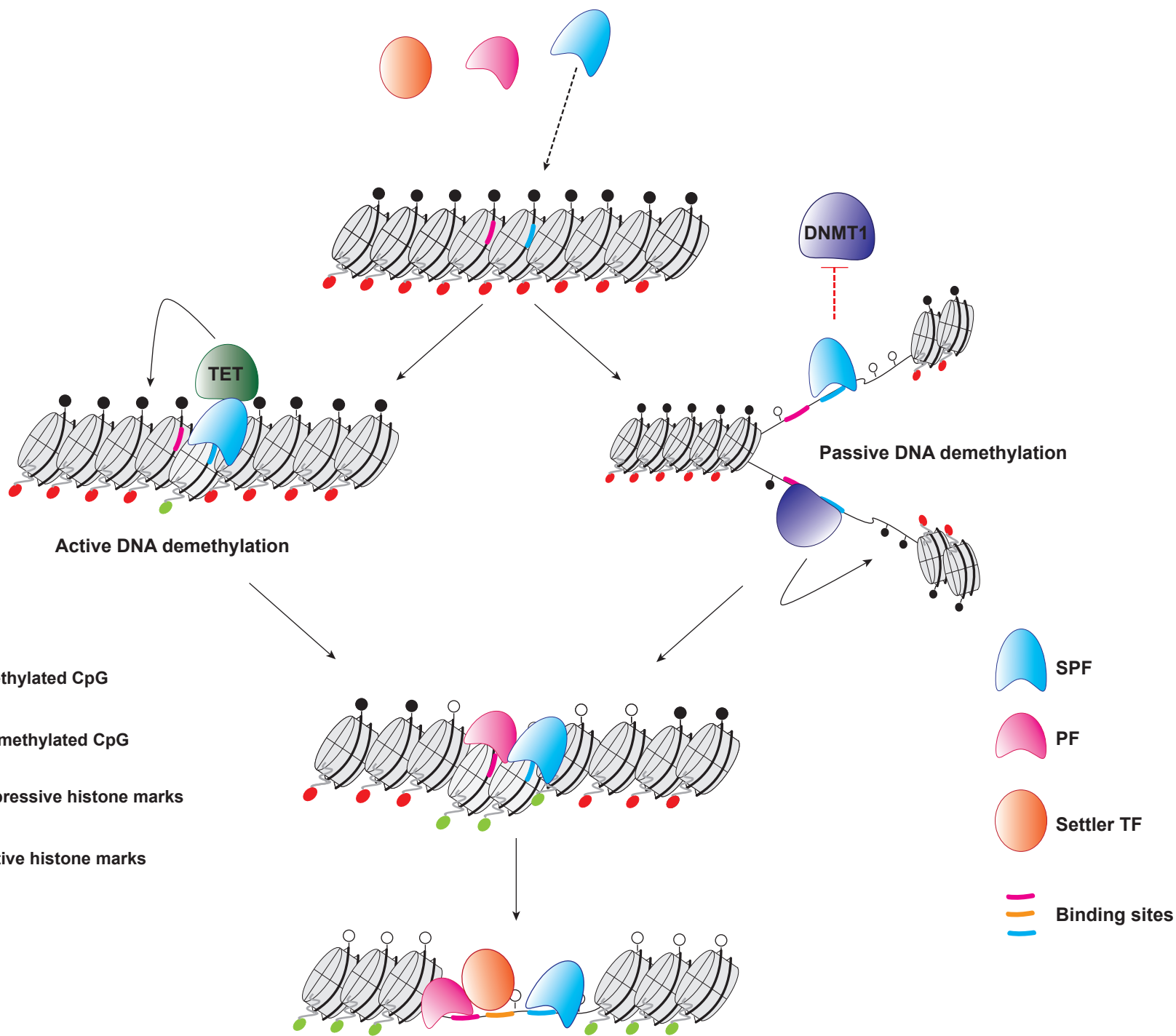
a**b****c****d**

Figure 6

a**Figure 7**